ESO Document Nr. E-TRE-UVA-222-0001
Issue 1.0 - 26 October 2010

UNIVERSIDAD DE VALPARAISO CHILE

Marc Sarazin

Digitally signed by Marc Sarazin
DN: cn=Marc Sarazin, o=ESO, ou=E-ELT, email=msarazin@eso.org, c=DE
Date: 2010.12.16 16:42:58 +01'00'

ADDENDUM: Measuring and forecasting PWV above La Silla, APEX and Paranal Observatories

Marta Caneo, Arlette Chacón, Lissette Cortes, Omar Cuevas, Michel Curé, Carolina Dougnac, Lizett Illanes, Julio Marín, Alejandra Oyanadel & Diana Pozo

Chapter 1

Introduction

The European Southern Observatory (ESO), in collaboration with the Institute for Space Imaging Science (ISIS) and the AstroMeteorology Group from the Universidad de Valparaíso, conducted a series of dedicated measurement campaigns to characterize the Precipitable Water Vapor (PWV) conditions over La Silla, Paranal and APEX (Atacama Pathfinder Experiment) observatories in northern Chile. Water vapor is the main source of opacity in infrared and radio (millimeter and sub-millimeter) spectral regions. These campaigns were performed using an Infrared Radiometer (IRMA), several medium and high-resolution spectrographs and a series of radiosondes launches conducted by the Astrometeorology group from Universidad de Valparaíso.

The first radiosondes campaign was held in May 2009 at La Silla observatory, located in the Coquimbo region. The second campaign was conducted in July 2009 at APEX observatory on Llano de Chajnantor, located in the Antofagasta region. The third and fourth campaigns were held at Paranal observatory, a site close to the coast at Antofagasta region, in July and August 2009 and November 2009, respectively.

The astrometeorology group use different tools to diagnose the PWV and predict its future values. One of the objectives of this study is to evaluate the PWV obtained from these tools with values measured by radiosondes. GOES-12 satellite data is used to estimate the PWV value at a specific location. The Weather Research and Forecasting (WRF) meteorological model, simulates the state of the atmosphere and forecast meteorological variables. PWV values can be obtained from WRF simulations over the domain of integration. In addition, the WRF model can be used to identify the synoptic patterns involved during those campaigns.

This study is part of the project "Study of Precipitable Water Vapor (PWV) at Llano de Chajnantor", number PO024344/GSER.

1.1 Main Objective

Measure and forecast the PWV above La Silla, APEX and Paranal Observatories.

1.2 Specific Objectives

- Measure the atmospheric vertical profile above La Silla, APEX and Paranal Observatories.
- Calculate the PWV from the vertical profiles.
- Evaluate the PWV estimated from GOES-12 satellite data.
- Implement the WRF meteorological model for the four radiosondes campaigns.
- Evaluate PWV forecasts calculated by WRF model.
- Analyze the synoptic conditions for the four radiosondes campaigns.

Chapter 2

Instrumentation

Radiosondes were used to measured the vertical profiles in the atmosphere. The equipment used were:

Vaisala Radiosonde RS92-SGP

This radiosonde model measures humidity, pressure, temperature and wind speed and direction.

Each radiosonde have a GPS receiver for wind finding, a silicon pressure sensor, heated twin humidity sensor and a small fast temperature sensor.

Vaisala Sounding Processing Subsystem SPS311

A fully digital telemetry link is implemented between the Vaisala Radiosondes RS92-SGP and the Vaisala Sounding Processing Subsystem SPS311. The SPS311's data reception technology makes extensive use of the software-defined radio technology. The radio signal is converted to fully digital format at very early phase of signal transmission, which improves performance in comparison with conventional analog receivers [1].

Ground Check Set GC25

This instrument check the functioning of the radiosonde, the sensors accuracy and set the frequency of the radiosonde.

Vaisala Portable Antenna Set CG31

Is a mobile antenna configuration designed to be used with GPS wind finding systems in the field conditions. The antenna set consists of Helix UHF antenna, GPS antenna and the Antenna Amplifier and Switch RAA111 on a tripod mount.

A PC with DigiCORA sounding software is needed. This software interconnects the Vaisala Sounding Processing Subsystem SPS311 (the Vaisala Portable Antenna Set CG31 is connected to this device) and the Ground Check Set GC25.

The steps made to launch all the radiosondes were the following:

1. Perform sounding preparation (calibrate the frequency, sensor and telemetry).
2. Prepare the balloon.
3. Connect the battery.
4. Launch the radiosonde.
5. Monitor the sounding with the DigiCora Sounding System.

Chapter 3

Radiosondes Campaigns

The AstroMeteorology group conducted four radiosondes launching campaigns in 2009. The different duties were: the operation of the radiosondes equipment, process the meteorological data from the vertical profile and make the corresponding report. The objective of these campaigns was the measurement of the PWV content in the atmosphere above La Silla, Paranal and APEX observatories.

All the campaigns were coordinated with the Institución de Aeronáutica Civil, which authorized all launches.

3.1 First Campaign: La Silla Observatory

The first campaign was held in La Silla observatory (altitude $\sim$ 2400 m, Figure 3.1) between May 5^{th} and 15^{th} of 2009. A number of 18 balloons were launched (Table 3.1). On May 13^{th} no data were recorded due to technical problems with the sensor.

3.2 Second Campaign: APEX

The second campaign was carried out in APEX telescope site in the Llano de Chajnantor (altitude $\sim$ 5100 m, Figure 3.1) between July 7^{th} and 11^{th} of 2009. On July 12^{th}, several logistic problems and bad weather caused the radiosonde launching location to be moved to APEX base camp Sequitor at a lower altitude ($\sim$ 2400 m). Table 3.2 shows the date and time of radiosonde launches.

La Silla Observatory campaign	
Date	Hour UTC
May 5^{th}, 2009	12:00
May 6^{th}, 2009	12:00
May 7^{th}, 2009	06:00
May 8^{th}, 2009	00:00 - 06:00
May 9^{th}, 2009	00:00 - 06:00 - 12:00
May 10^{th}, 2009	00:00 - 06:00
May 11^{th}, 2009	00:00 - 06:00
May 12^{th}, 2009	00:00
May 13^{th}, 2009	00:00
May 14^{th}, 2009	00:00 -12:00
May 15^{th}, 2009	00:00 - 06:00

Table 3.1: Schedule of radiosondes launches at La Silla Observatory.

Figure 3.1: Map locations of each observatory where the radiosonde campaigns were performed.

APEX radiosonde campaign	
Date	Hours UTC
July 7th, 2009	00:00 - 12:00
July 8th, 2009	00:20 - 12:00
July 9th, 2009	00:00 - 12:40
July 10th, 2009	00:00 - 12:07
July 11th, 2009	00:00 - 12:20
July 12th, 2009	00:00 - 12:45
July 13th, 2009	00:00 - 12:00
July 14th, 2009	00:00 - 13:15
July 15th, 2009	00:11 - 12:00
July 16th, 2009	00:00 - 12:00

Table 3.2: Schedule of radiosondes launches at APEX observatory.

3.3 Third Campaign: Paranal Observatory

The third campaign was conducted at Paranal Observatory ($\sim$ 2600 m, Figure 3.1) from July 28^{th} to August 10^{th}, 2009. Table 3.3 shows the dates and times of radiosonde launches. No launching was made on July 28^{th} due to problems with helium supply.

Paranal Observatory radiosonde campaign	
Date	Hours UTC
July 29^{th}, 2009	12:00
July 30^{th}, 2009	12:15
July 31^{th}, 2009	00:30 - 12:00
August 1^{st}, 2009	00:00 - 06:15 - 12:00
August 2^{nd}, 2009	00:00 - 06:15
August 3^{rd}, 2009	00:00
August 4^{th}, 2009	00:00
August 5^{th}, 2009	01:00 - 06:00
August 6^{th}, 2009	01:00 - 06:15
August 7^{th}, 2009	00:00 - 06:20 -12:00
August 8^{th}, 2009	00:00 - 06:00
August 9^{th}, 2009	00:00
August 10^{th}, 2009	01:10 - 12:00

Table 3.3: Schedule of radiosondes launches at Paranal Observatory.

3.4 Fourth Campaign: Paranal Observatory

This was the second campaign conducted at Paranal Observatory from November 9^{th} to 19^{th}, 2009. Table 3.4 presents the schedule of radiosondes launching.

Paranal Observatory radiosonde campaign	
Date	Hours UTC
November 9^{th}, 2009	12:00
November 10^{th}, 2009	12:00
November 11^{th}, 2009	00:00 - 06:00 - 12:00
November 12^{th}, 2009	00:00 - 06:00 - 12:15
November 13^{th}, 2009	00:00 - 06:00 - 12:00
November 14^{th}, 2009	00:00 - 06:00 - 12:00
November 15^{th}, 2009	00:00 - 06:00 - 12:20
November 16^{th}, 2009	00:00 - 06:15 - 12:00
November 17^{th}, 2009	00:00 - 06:05 - 12:00
November 18^{th}, 2009	00:00 - 06:00 -12:00
November 19^{th}, 2009	00:00 - 06:00 - 12:00

Table 3.4: Schedule of second radiosondes launches at Paranal Observatory.

Chapter 4

Methodology & Statistics

The equation used to calculate the PWV from radiosondes and WRF model was:

$$PWV = \frac{1}{g}\int_{P1}^{P2} x dp \tag{4.1}$$

where g is the acceleration of gravity, $x(P)$ is the water vapor mixing ratio at a given pressure level P, and PWV provides the water vapor that could condensate in a layer bounded by pressures p1 and p2.

Several statistical parameters were used to validate the PWV calculated from WRF model and GOES-12:

Root Mean Squared Error

The root mean square error is defined as:

$$RMSE = \sqrt{\sum_{i=1}^{N} \frac{(y_i - x_i)^2}{N}}$$

where y_i is the value of the meteorological variable predicted by the model, x_i is the meteorological value measured by the radiosonde and N is the total number of data analyzed.

The root mean square error for the wind direction is defined as:

$$RMSE_{Dir} = \sqrt{\sum_{i=1}^{N} \frac{D^2}{N}}$$

$$D = min\left(|y_i - x_i|, |360 - (y_i - x_i)|\right)$$

where y_i is the value of the wind direction predicted by the model, x_i is the wind direction measured by the radiosonde and N is the total number of data analyzed.

BIAS

The bias provides information on the trend of the model to overestimate or underestimate a variable. It quantifies the systematic error in the models and is defined as:

$$BIAS = \sum_{i=1}^{N} \frac{(y_i - x_i)}{N}$$

where y_i is the value of the meteorological variable predicted by the model, x_i is the meteorological value measured by the radiosonde and N is the total number of data analyzed.

The bias for the wind direction is defined as:

$$BIAS_{Dir} = \sum_{i=1}^{N} \frac{D}{N}$$

if $y_i < x_i$

$D = y_i - x_i$ if $|y_i - x_i| < |360 + (y_i - x_i)|$

$D = 360 + (y_i - x_i)$ if $|y_i - x_i| > |360 + (y_i - x_i)|$

if $y_i > x_i$

$D = y_i - x_i$ if $|y_i - x_i| < |(y_i - x_i) - 360|$

$D = (y_i - x_i) - 360$ if $|y_i - x_i| > |(y_i - x_i) - 360|$

where y_i is the value of the meteorological variable predicted by the model, x_i is the meteorological value measured by the radiosonde and N is the total number of data analyzed.

Correlation

We calculate the correlation between observed and predicted values to determine the performance of the model. The equation that defines the correlation is:

$$Corr = \frac{\sum_{i=1}^{N}(x_i - \overline{x}) \bullet \sum_{i=1}^{N}(y_i - \overline{y})}{\sqrt{\sum_{i=1}^{N}(x_i - \overline{x})^2 \bullet \sum_{i=1}^{N}(y_i - \overline{y})^2}}$$

where y_i is the value of the meteorological variable predicted by the model, x_i is the meteorological value measured by the radiosonde, $\overline{y}$ is the average of the meteorological variable predicted

by the model, $\overline{x}$ is the average of the meteorological variable measured by the radiosonde and N is the total number of data analyzed.

Cumulative distribution function (CDF)

The Cumulative Distribution Function F(x) describes the probability that a random variable X will be found at a value less than or equal to x. Specifically:

$$F(x) = P\left(\{X \leq x\}\right) = \sum_{t<x} f(t)$$

For more information, see Mathematical Statistics with Applications [3].

Chapter 5

Evaluation of GOES-12

PWV values from GOES-12 were obtained using the methodology described in the Section 3 of our final report: "Study of Precipitable Water Vapor (PWV) at Llano de Chajnantor". In this methodology temperature and relative humidity vertical profiles from FNL analyses [5] were used to calculate the PWV from GOES-12. PWV values calculated from FNL and from GOES-12 were validated against those calculated from radiosondes.

This methodology was developed for Llano de Chajnantor, specifically for APEX observatory. For this reason, all necessary changes in the methodology were made to implement it in La Silla and Paranal sites.

5.1 First Campaign: La Silla Observatory

Figure 5.1 shows the time series of PWV for La Silla site. GOES-FNL overestimates by more than 1.5 mm the PWV calculated from radiosondes and the FNL analysis presents a underestimation of -0.11 (Table 5.1). In regard to data dispersion FNL shows a lower error (1.18 mm) than GOES-FNL (2.32 mm).

Cumulative distribution functions (CDF) show that 25% of PWV from FNL shows an error $<$ 0.38 mm while GOES-FNL shows an error $<$ 1.06 mm. Furthermore, 95% of FNL data and GOES-FNL have errors $<$ 2.59 mm and 5.32 mm, respectively.

SP/Observatory	La Silla		APEX		
	GOES-FNL	FNL	GOES-FNL	FNL	Rad
Corr	0.81	0.78	0.93	0.96	0.99
BIAS	1.89	-0.11	0.39	0.31	0.13
RMSE	2.32	1.18	0.47	0.55	0.56

SP/Observatory	Paranal (1)		Paranal (2)	
	GOES-FNL	FNL	GOES-FNL	FNL
Corr	0.25	0.76	-0.20	0.04
BIAS	1.68	1.29	3.25	1.35
RMSE	2.11	1.55	3.73	1.75

Table 5.1: Statistics parameters of GOES-FNL and the FNL analysis for the four radiosondes campaigns.

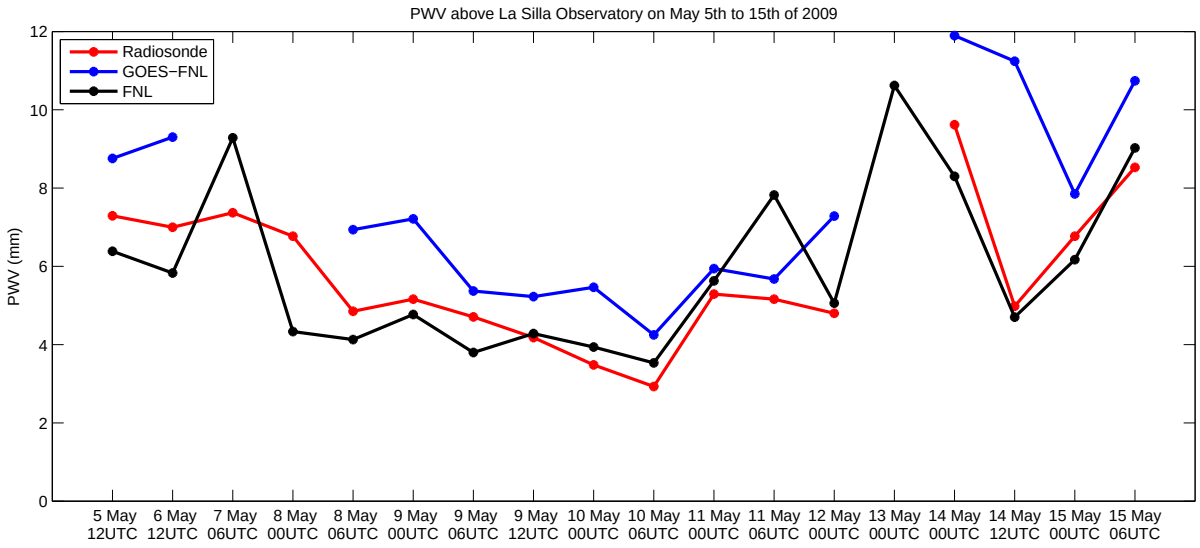

Figure 5.1: Time series of PWV for the First Campaign at La Silla. The red line represents the PWV measured by radiosondes, blue line GOES-FNL and the black line is the FNL analysis.

5.2 Second Campaign : APEX Observatory

For this site, we includes PWV values from APEX radiometer to the comparison. Figure 5.2 shows that GOES-FNL and FNL analysis have the same tendency than that shown by radiosondes but overestimate it by less than 0,5 mm (Table 5.1). The same performance is

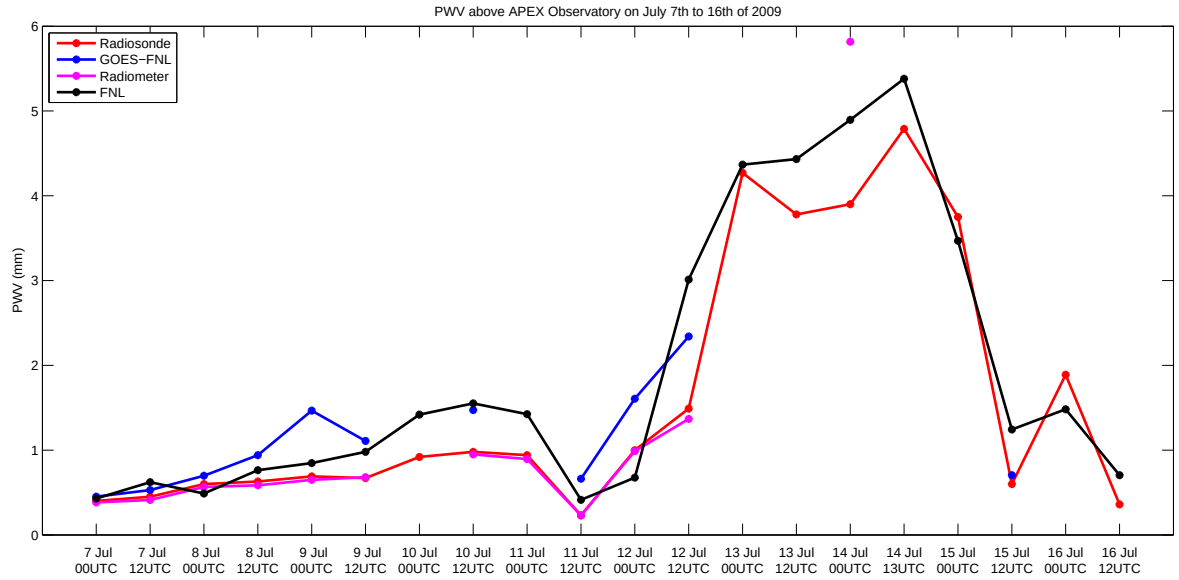

Figure 5.2: Time series of PWV for the Second Campaign at APEX. The red line represents the PWV measured by radiosondes, the magenta line is the radiometer, the blue line GOES-FNL and the black line is the FNL analysis.

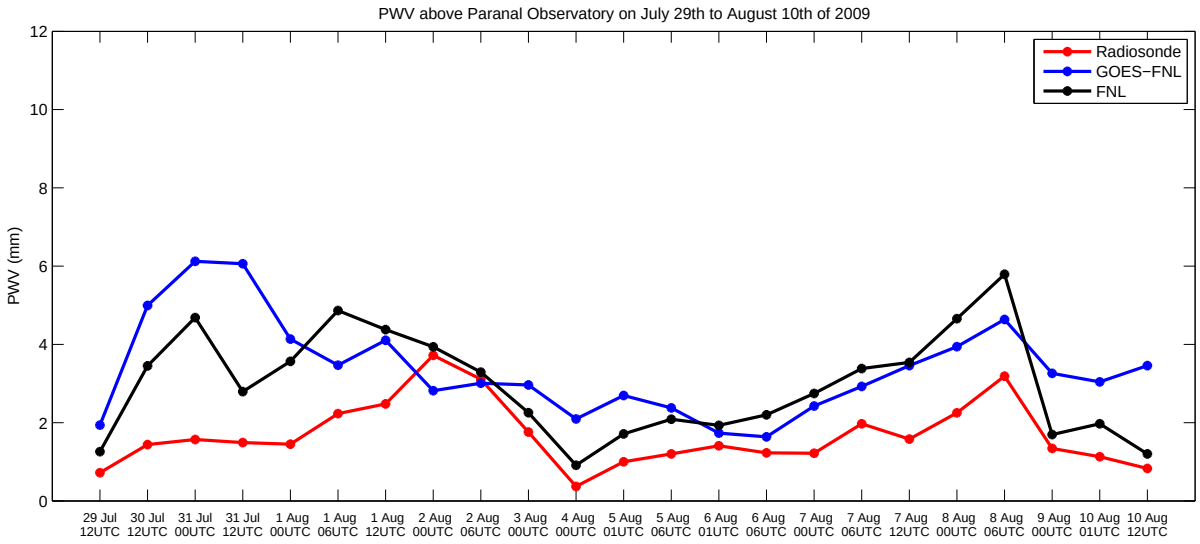

Figure 5.3: Time series of PWV for the Third Campaign at Paranal. The red line represents the PWV measured by radiosondes, blue line GOES-FNL and the black line is the FNL analysis.

with the radiometer but the overestimation is less than 0.2 mm and the correlation is 0.99 (Table 5.1).

In figure 5.2 there are some missing values in the graphic. This is because the methodology used can not calculate PWV when clouds are present. In those days, the synoptic condition was a Cut-off Low (CL) with presence of clouds (section 7.2.2).

5.3 Third Campaign: Paranal Observatory

PWV values from GOES-FNL and FNL analysis overestimate the PWV from radiosondes all days. However, they show the same tendency than observations from August 2^{nd} to the end of the campaign (Figure 5.3). FNL shows the best correlation (0.76) and lowest error ($<$ 1.60 mm) with observations (Table 5.1) and 95% of FNL and GOES-FNL data have errors less than 2.80 mm and 4.56 mm, respectively.

5.4 Fourth Campaign: Paranal Observatory

In the second PWV measurements campaign at Paranal, GOES-FNL shows a large overestimation observations (Figure 5.4), showing a BIAS of 3.25 mm, a RMSE of 3.73 mm and correlation of -0.20. On the other hand, the FNL analysis presents values of BIAS and RMSE lower than 2 mm, and not correlation at all (Table 5.1) and 25% of its data shows an error less than 0.45 mm, 50% has an error $<$ 1.48 mm and the 75% present an error $<$2.17 mm.

The evaluation of GOES-FNL at the three study sites indicates that the best performance is obtained at APEX observatory, showing the same tendency than radiosondes and low mean BIAS ($<$ 0.54 mm). The largest errors were observed during the second campaign at Paranal with values more than 3 mm.

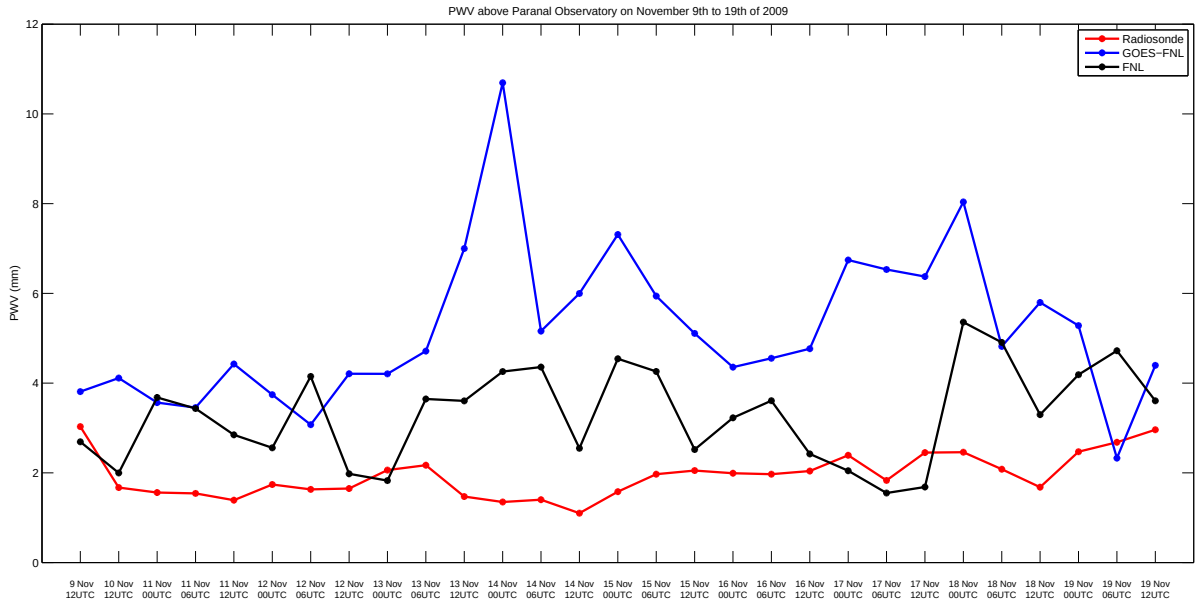

Figure 5.4: Time series of PWV for the Fourth Campaign at Paranal. The red line represents the PWV measured by radiosondes, blue line GOES-FNL and the black line is the FNL analysis.

Chapter 6

Evaluation of WRF Model

The WRF model validation was performed comparing data from domain 4 (highest resolution ∼1 km) with radiosondes. Section 6.1 will present the results from the PWV comparison and section 6.2 will show the vertical profiles comparison of temperature, relative humidity, mixing ratio, wind speed and direction.

6.1 Validation of PWV

The WRF model simulations were run 72 hours every day during the periods of radiosonde campaigns (Tables 3.1, 3.2, 3.3 and 3.4). Radiosondes were launched at just 00, 06 and 12 UTC in each campaign. Since the WRF model performance during the 72 hours of forecasts was evaluated everyday, simulations were compared with radiosondes at 00, 06, 12 UTC for the first day, at 24, 30 and 36 forecast hours for the second day and at 48, 54 and 60 forecast hours for the third day.

6.1.1 First Campaign: La Silla Observatory

The first PWV campaign was conducted at La Silla site. Figure 6.1 shows a time-series comparison between the PWV measured by the radiosonde and the PWV calculated by the WRF model. In this figure, the values extracted from the WRF model overestimate the PWV by more than 2 mm. Table 6.1 shows the errors for the three days of forecast, where the second day of forecast present the lowest error, with RMSE and BIAS of 2.80 mm and 2.48 mm, respectively. The CDF function shows that 50% of forecasts from the second day presents an error bias less than 2.3 mm. A possible explanation of why the second day of forecasts shows

the best agreement with observations could be the fact that the model may need some time for stabilization but this should be further investigated.

SP/Observatory	La Silla			APEX		
Forecast (hrs)	00-06-12	24-30-36	48-54-60	00-06-12	24-30-36	48-54-60
Corr	0.91	0.80	0.83	0.93	0.93	0.93
BIAS	2.72	2.48	2.97	0.13	0.13	0.15
RMSE	2.92	2.80	3.23	0.56	0.60	0.60
SP/Observatory	Paranal (1)			Paranal (2)		
Forecast (hrs)	00-06-12	24-30-36	48-54-60	00-06-12	24-30-36	48-54-60
Corr	0.82	0.71	0.66	0.48	0.61	0.31
BIAS	1.47	1.68	1.93	2.43	2.09	2.35
RMSE	1.66	1.88	2.29	2.53	2.27	2.52

Table 6.1: Statistics parameters (BIAS, RMSE & Corr) for the four radiosondes campaigns.

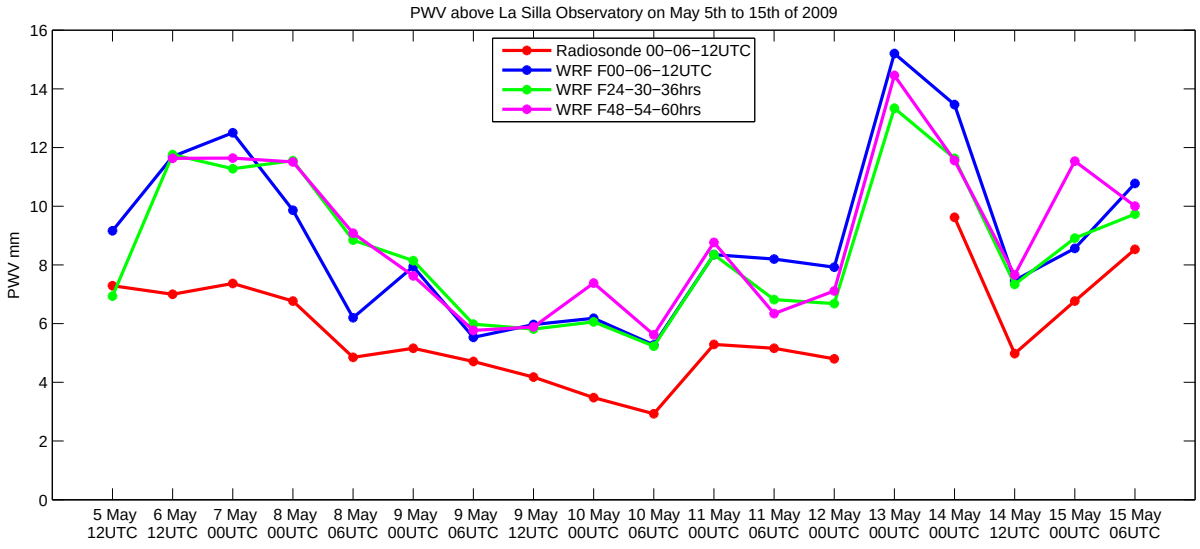

Figure 6.1: Comparison of PWV measured by the radiosonde and the PWV from WRF model for La Silla Observatory.

6.1.2 Second Campaign: APEX Observatory

The second PWV campaign was conducted at APEX Observatory. As mentioned in section 3.2, the location where radiosondes were launched moved to San Pedro de Atacama in the middle of APEX campaign. However, the analysis was focused on APEX location.

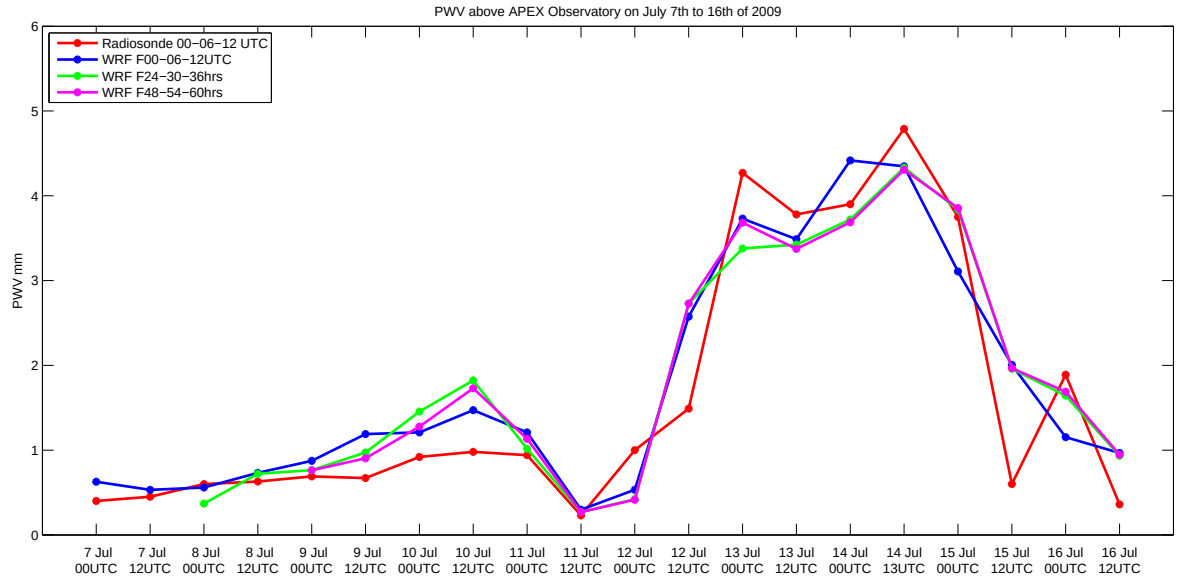

Figure 6.2: Comparison of PWV measured by the radiosonde and the PWV from WRF model for APEX Observatory.

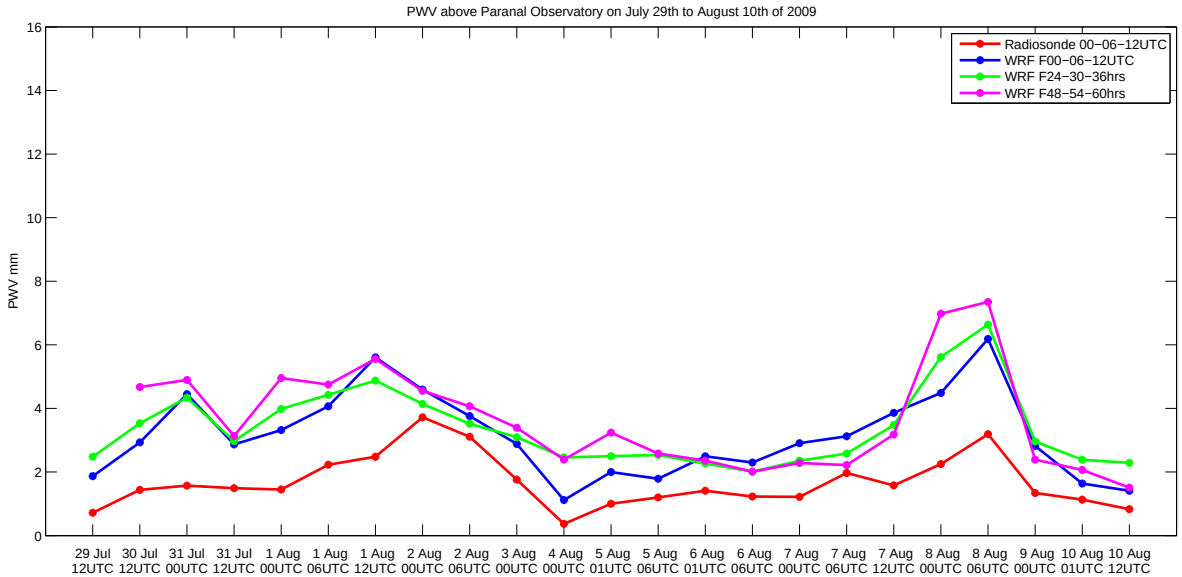

Figure 6.3: Comparison of PWV measured by the radiosonde and the PWV from WRF model for Paranal Observatory.

Figure 6.2 shows a very good agreement between values simulated by the WRF model and those calculated from radiosondes. During the three days of forecasts, the PWV is slightly overestimated by no more than 0.15 mm, with average RMSE of 0.6 mm and a correlation of 0.93 (Table 6.1). The CDF functions indicate that errors are less than 0.58 mm in 75% of data. The performance of the model at this site is good, probably caused by the high altitude where it is located ($\sim$ 5.100 m) and the very dry atmospheric conditions that predominate over the year.

6.1.3 Third Campaign: Paranal Observatory

The third PWV campaign was conducted at Paranal site, in mid-winter season. Figure 6.3 shows that PWV from WRF model overestimates the radiosondes by more than 1 mm during the three days of forecasts (Table 6.1). Table 6.1 shows that the lowest RMSE and BIAS is observed in the first day of forecast, where CDF functions indicate that 50% and 75% of data show errors less than 1.15 mm and 1.86 mm, respectively.

6.1.4 Fourth Campaign: Paranal Observatory

The fourth campaign was conducted at Paranal but during the spring season (November). The objective of this last campaign was to obtain the PWV for this site during different seasons.

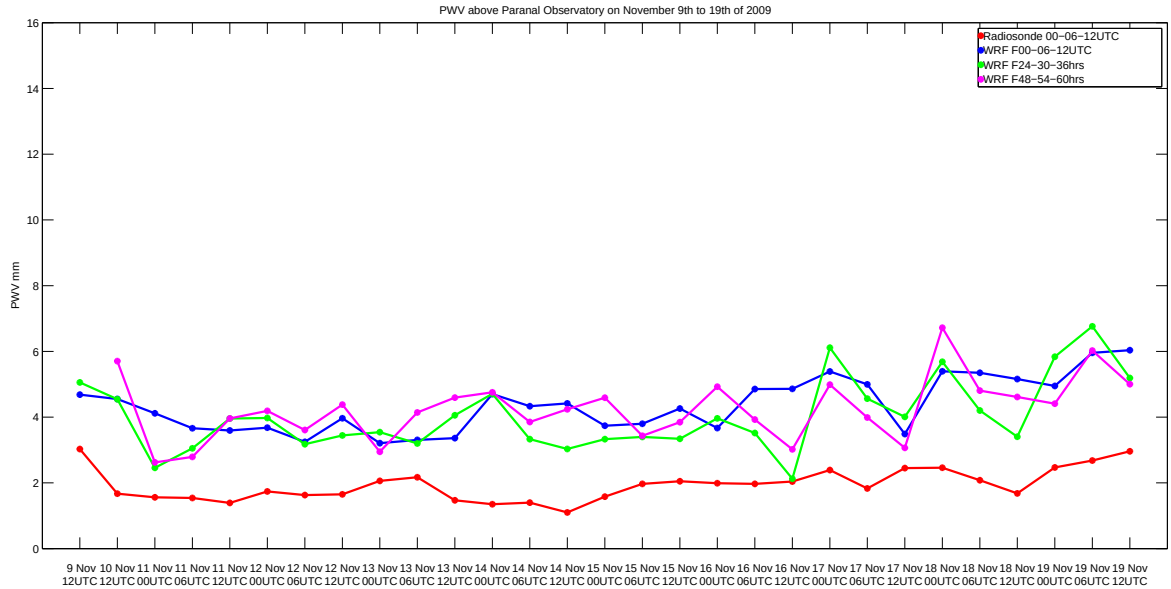

Figure 6.4: Comparison of PWV measured by the radiosonde and the PWV from WRF model for Paranal Observatory.

The performance of the WRF model is not as good as that obtained in the third campaign. Figure 6.4 indicates that the model does not show the same tendency than radiosondes and overestimates the PWV value by more than 2 mm (Table 6.1). This site also shows the lowest RMSE and BIAS during the second day of forecasts with the largest correlation. The CDF function for the second day of forecast shows the largest number of data with small errors (50% of data with errors less than 1.9 mm). The comparison of WRF simulations during two different seasons in Paranal may suggest that the model can better predict the cold season than the warm season but this supposition should be further investigated.

The WRF model overestimates the time evolution of PWV during La Silla and both Paranal campaigns all though it shows the same tendency than observations. A possible source of error in this comparison could be the fact that geographical coordinates used to extract the values from the WRF model are not the same were the radiosondes were launched. This difference is not presented in APEX site because the launches were made very close to the antenna (geographical coordinate used in the WRF model).

6.2 Evaluation of Vertical Profiles

WRF vertical profiles were extracted using a bilineal interpolation to select the point where each campaign took place. An average profile for WRF simulations and radiosondes were calculated and used for comparison. Vertical profiles of temperature, relative humidity, water vapor mixing ratio, wind speed and direction were evaluated.

The temperature vertical profiles from WRF are similar to the profiles measured by the radiosondes (Figures 6.5 & 6.6). The RMSE are larger than 1^{o}C between 750 hPa and 600 hPa at La Silla and Paranal. The model underestimates temperature between these pressures during the first, third and fourth campaigns (La Silla and Paranal). However, at APEX, the model mostly overestimates temperature, but by less than 1^{o}C (Figure 6.5b).

The comparison between relative humidity profiles shows that the RMSE is less than 20% below 300 hPa (Figures 6.7 & 6.8) although the third and fourth campaigns show errors less than 10%. Both campaigns conducted at Paranal site present a good agreement at middle pressure levels where the RMSE is near 0 (Figure 6.8). Above 300 hPa, the model overestimates the relative humidity values at all campaigns.

The vertical profiles of mixing ratio are used to calculate the PWV value using equation 4.1. The WRF overestimates the mixing ratio vertical profiles in the four campaigns (Figures 6.9 & 6.10). The best simulation of this variable were performed over the APEX site (Figure 6.9b)

with RMSE between 0 and 0.5 mm. This may be due to the very dry conditions present at that site. The largest errors are found below 600 hPa with RMSE as large as 2 g/g in the fourth campaign (Figure 6.10b).

Figures 6.11 and 6.12 show the vertical profiles of wind speed. In the four campaigns the average WRF vertical profile shows the same tendency than that from radiosondes. The best performance was obtained at APEX site and at the second campaign over Paranal site, with RMSE less than 2 m/s (except at upper pressure levels in APEX). The presence of the Jet Stream is indicated at upper pressure levels over APEX and Paranal (both campaigns). The WRF model reproduces the Jet Stream but underestimates its value by 1.5 m/s in APEX and the second Paranal campaign and by 4 m/s during the first Paranal campaign.

In the case of wind direction vertical profiles (Figures 6.13 & 6.14), the agreement between the model and radiosondes is very good, except below 700 hPa at the second campaign in Paranal site where WRF shows RMSE larger than 60^{o} and around 600 hPa in La Silla with RMSE near 45^{o}.

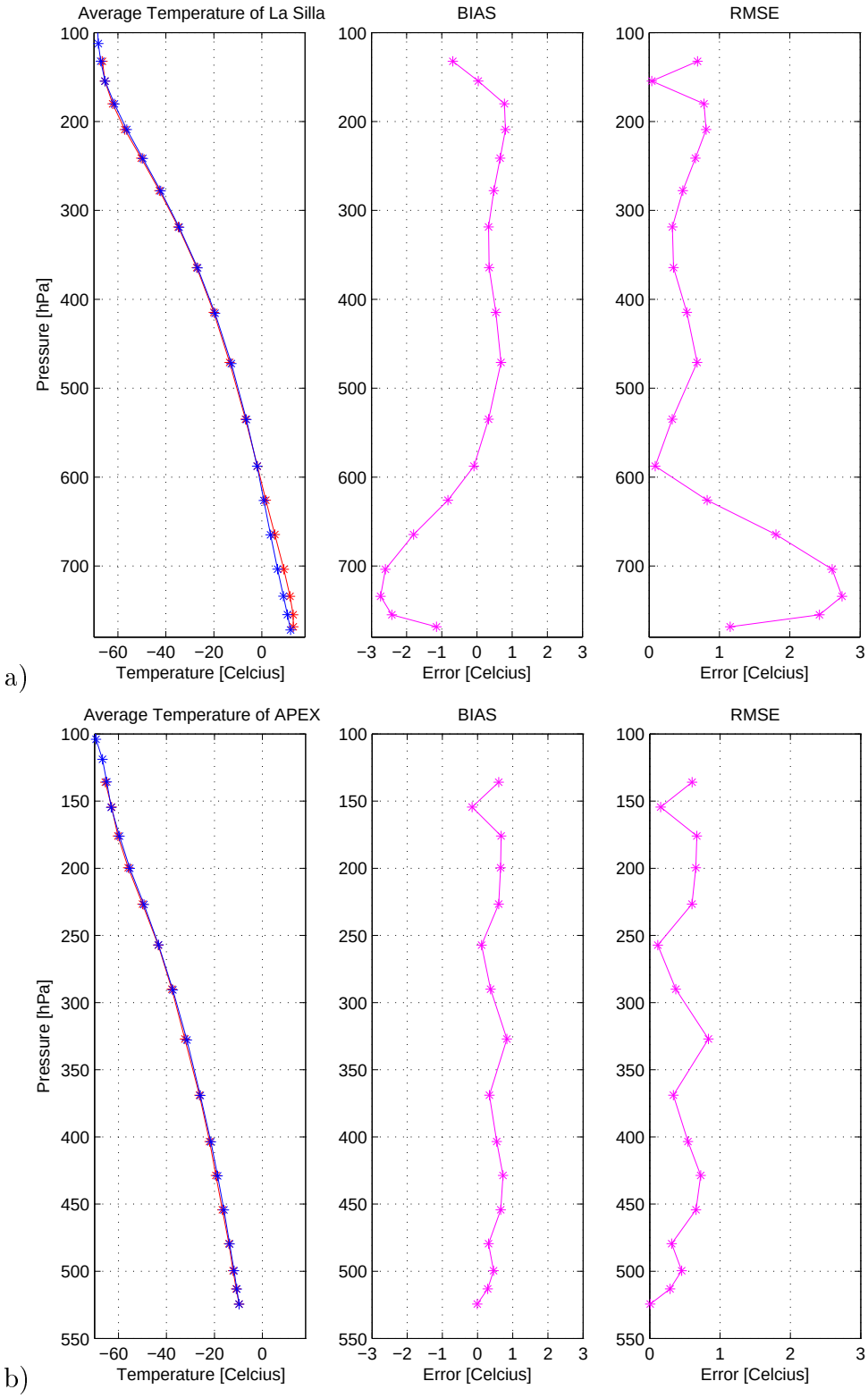

Figure 6.5: Mean vertical profiles of temperature for radiosondes (red line) and WRF model (blue line) (first box), vertical profiles of BIAS (second box) and RMSE (third box) during a) La Silla campaign and b) APEX campaign.

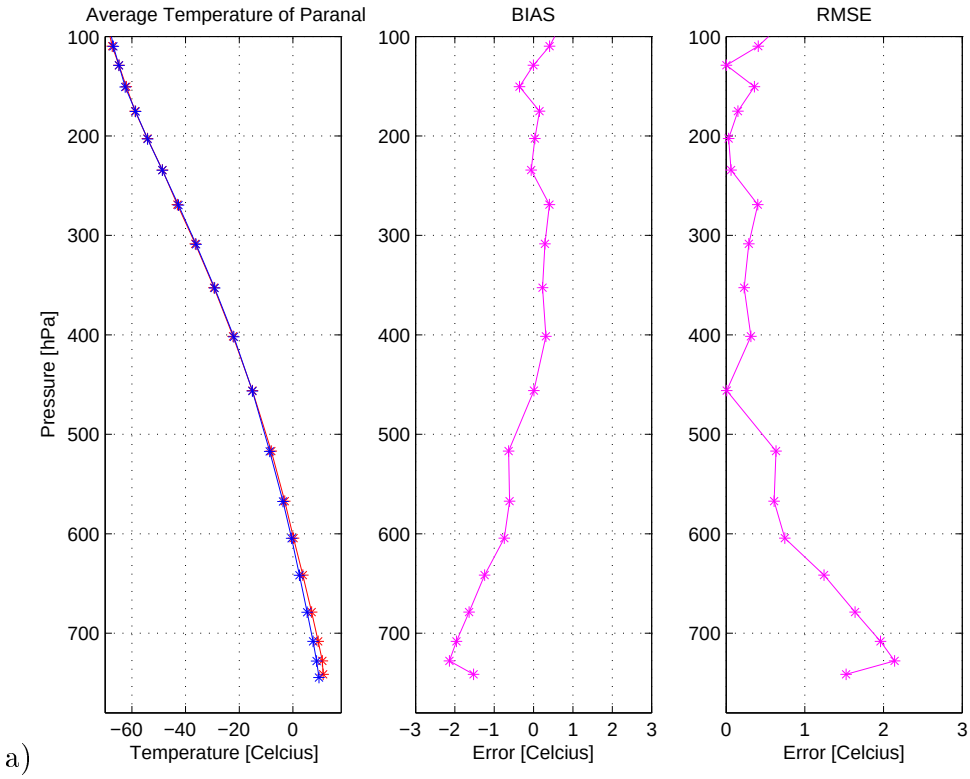

Figure 6.6: Mean vertical profiles of temperature for radiosondes (red line) and WRF model (blue line) (first box), vertical profiles of BIAS (second box) and RMSE (third box) during a) the first Paranal campaign and b) the second Paranal campaign.

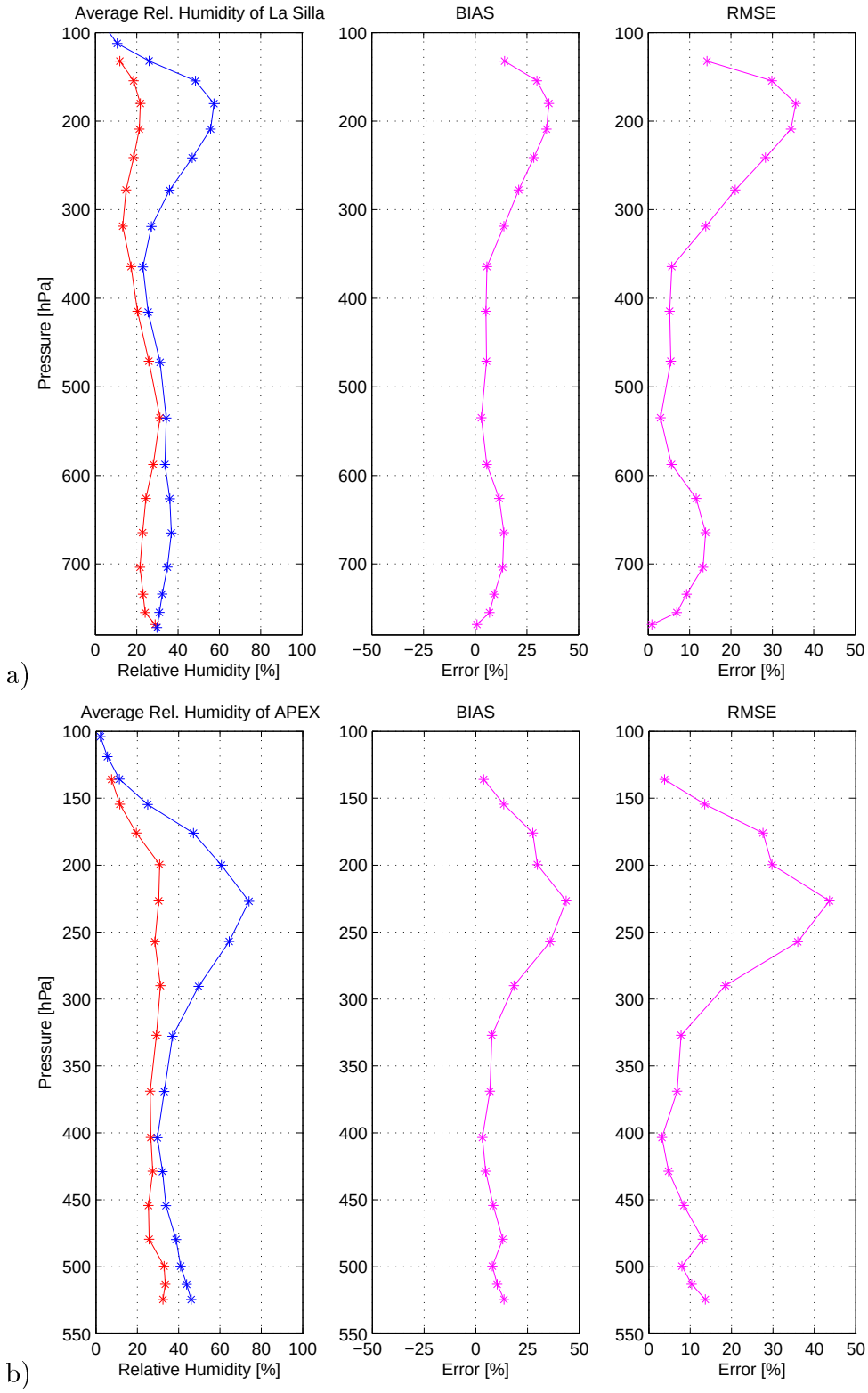

Figure 6.7: Mean vertical profiles of relative humidity for radiosondes (red line) and WRF model (blue line) (first box), vertical profiles of BIAS (second box) and RMSE (third box) during a) La Silla campaign and b) APEX campaign.

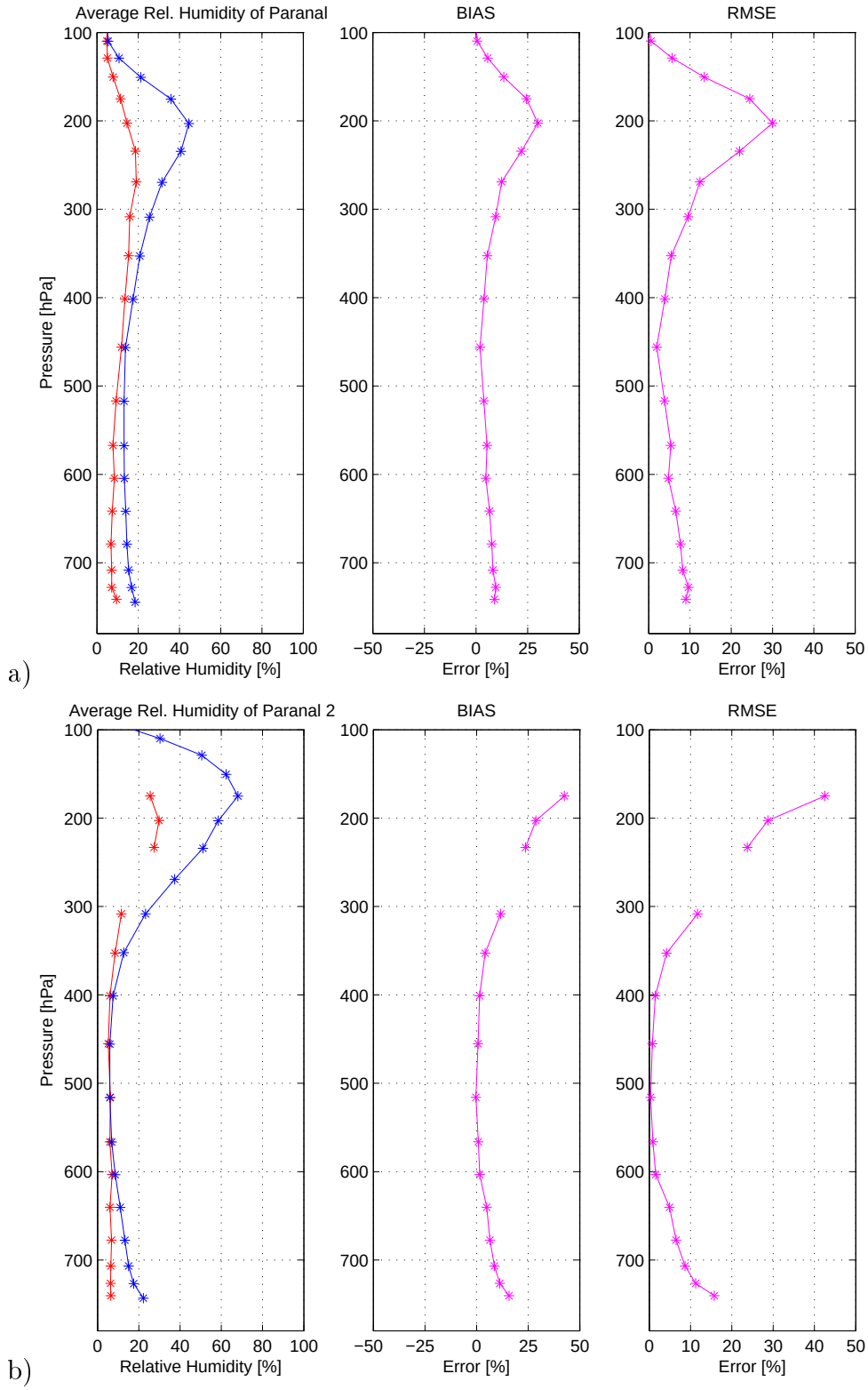

Figure 6.8: Mean vertical profiles of relative humidity for radiosondes (red line) and WRF model (blue line) (first box), vertical profiles of BIAS (second box) and RMSE (third box) during a) the first Paranal campaign and b) the second Paranal campaign.

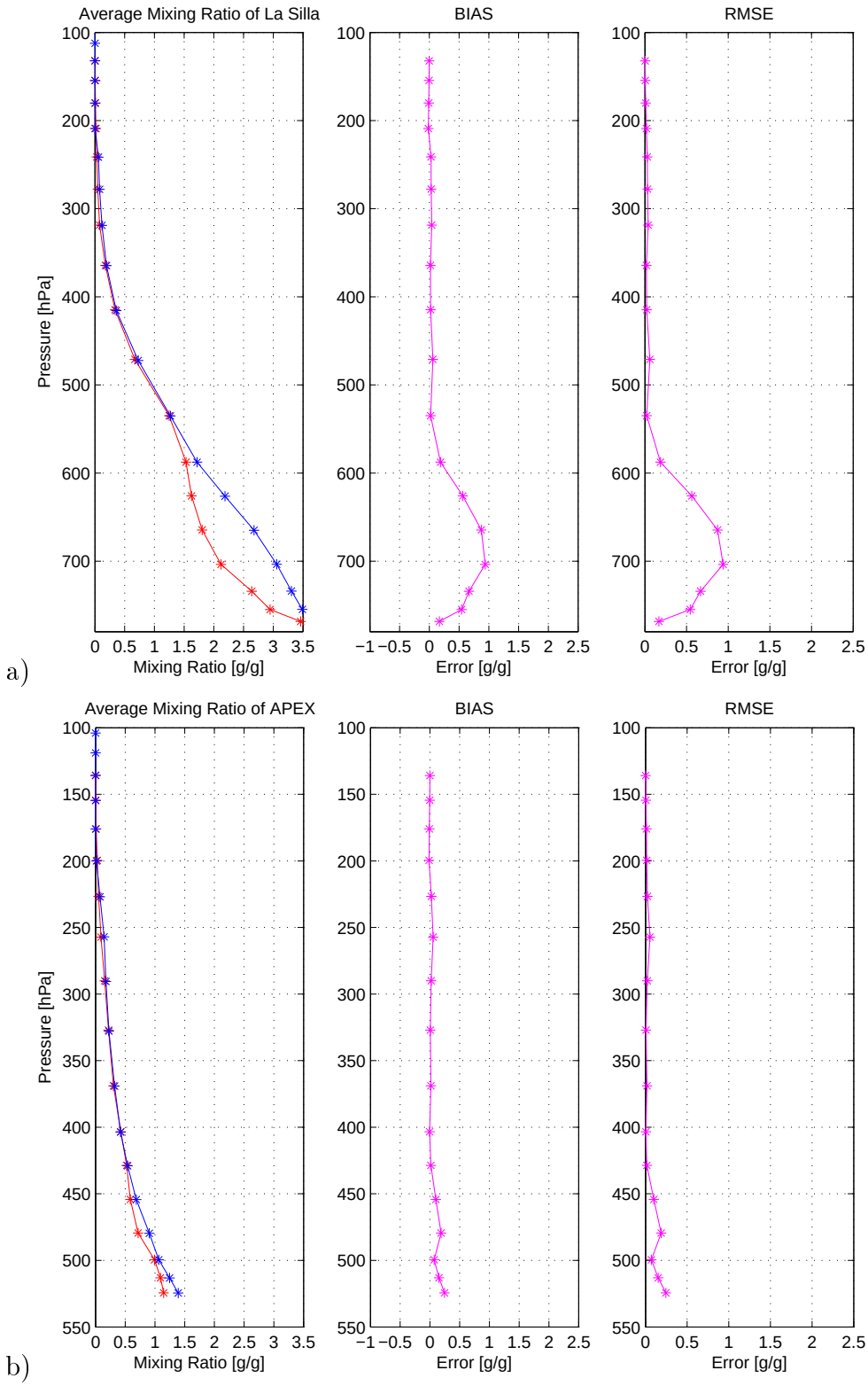

Figure 6.9: Mean vertical profiles of mixing ratio for radiosondes (red line) and WRF model (blue line) (first box), vertical profiles of BIAS (second box) and RMSE (third box) during a) La Silla campaign, and b) APEX campaign.

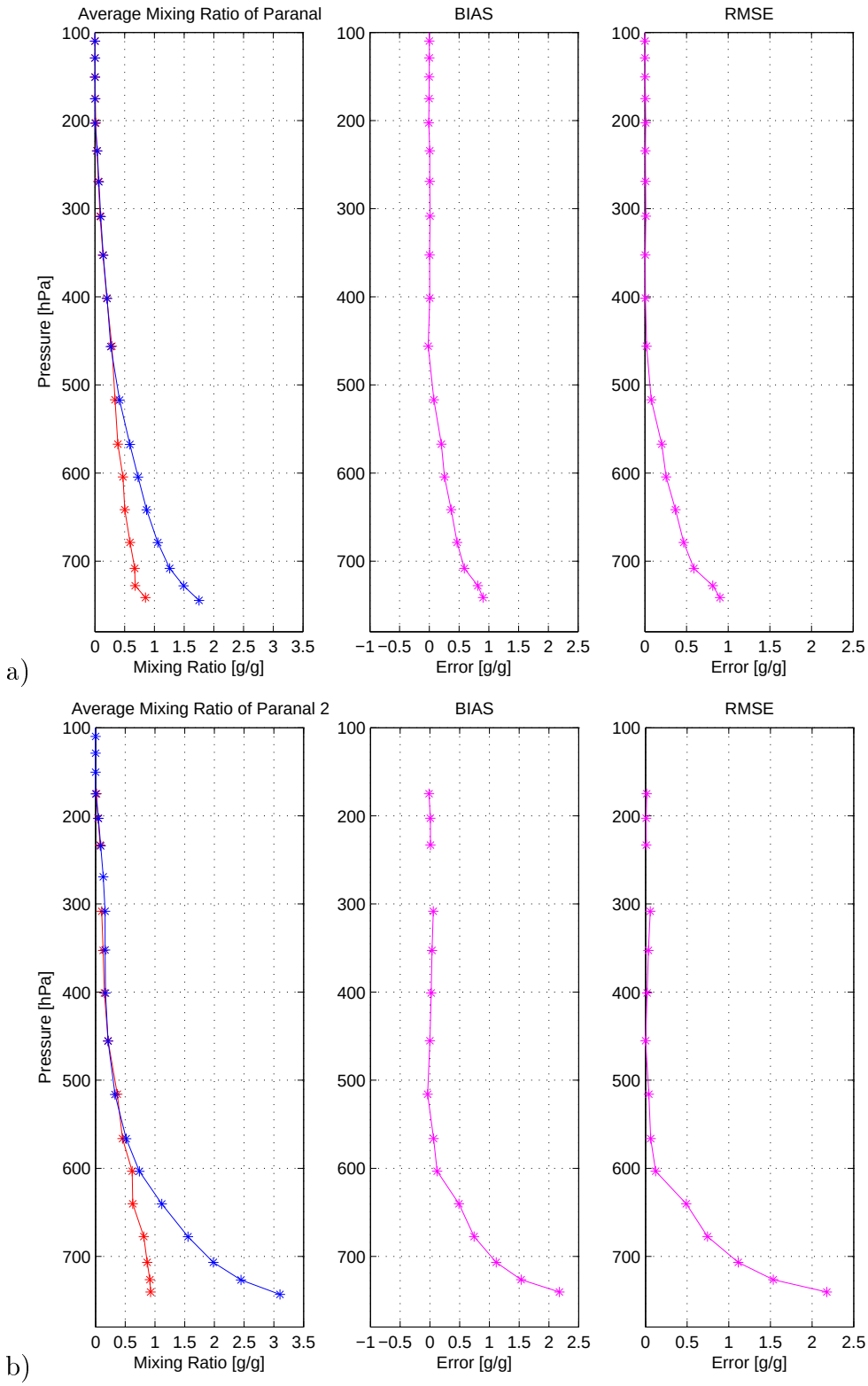

Figure 6.10: Mean vertical profiles of mixing ratio for radiosondes (red line) and WRF model (blue line) (first box), vertical profiles of BIAS (second box) and RMSE (third box) during a) the first Paranal campaign and b) the second Paranal campaign.

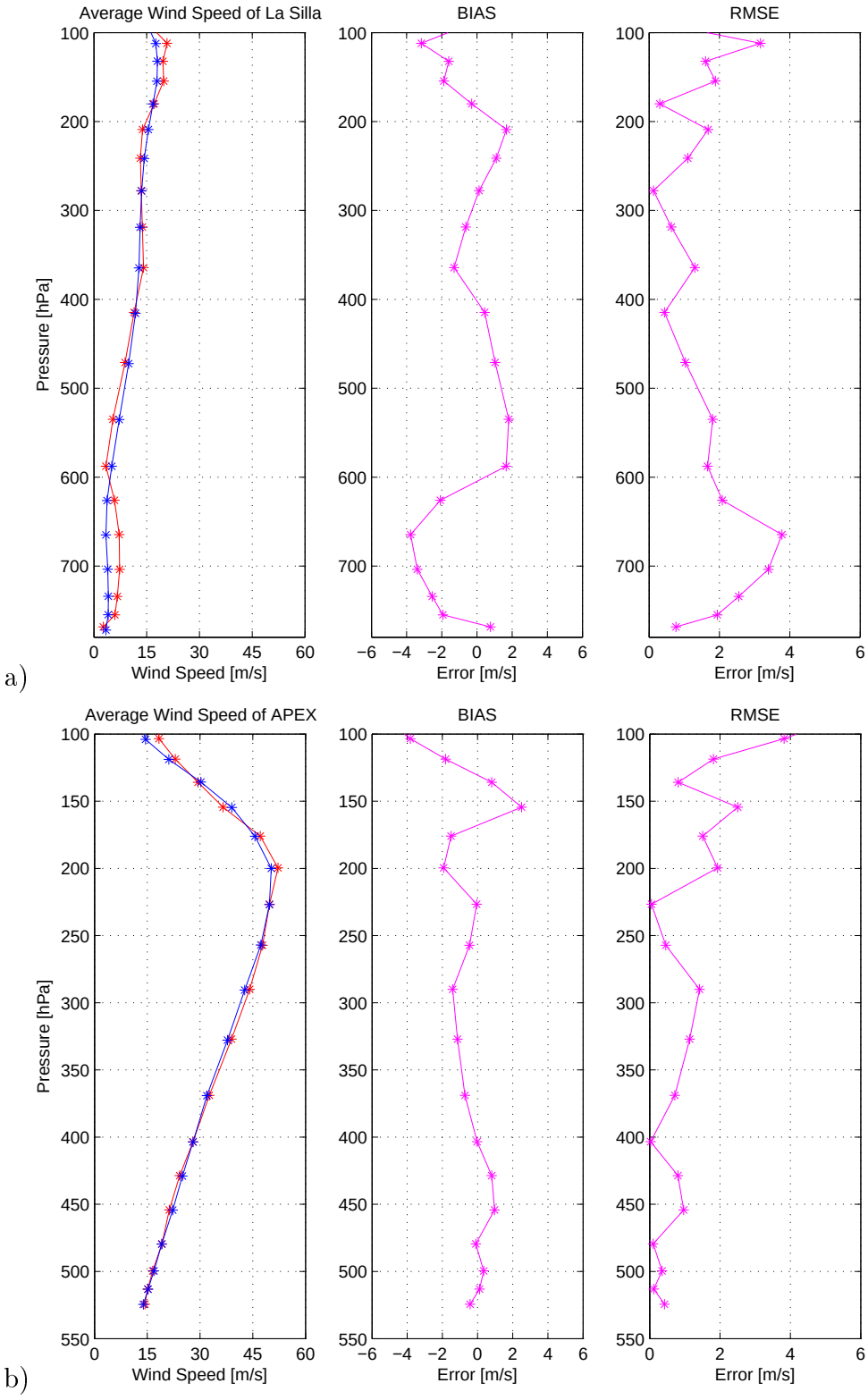

Figure 6.11: Mean vertical profiles of wind speed for radiosondes (red line) and WRF model (blue line) (first box), vertical profiles of BIAS (second box) and RMSE (third box) during a) La Silla campaign and b) APEX campaign.

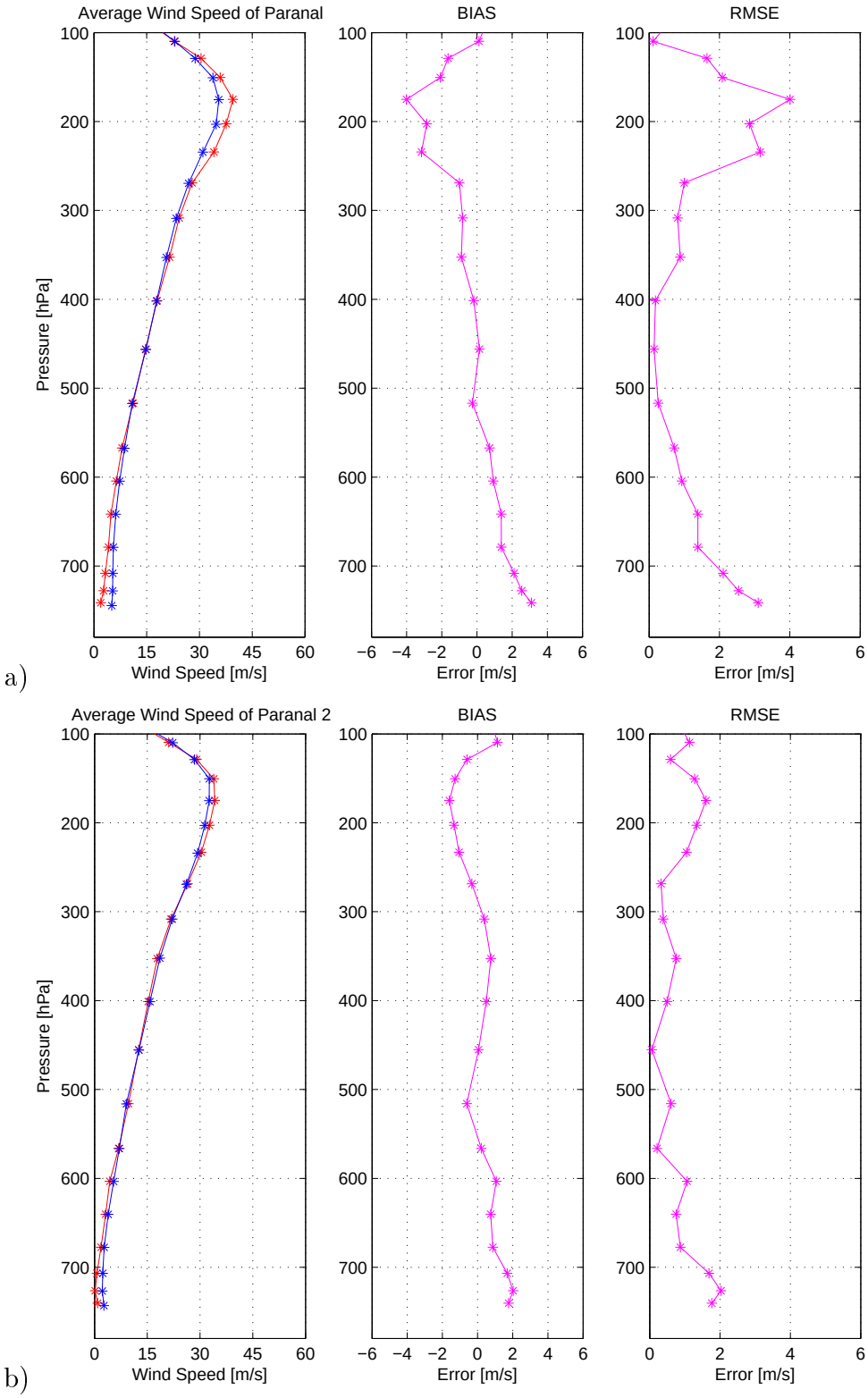

Figure 6.12: Mean vertical profiles for wind speed of radiosondes (red line) and WRF model (blue line) (first box), vertical profiles of BIAS (second box) and RMSE (third box) during a) the first Paranal campaign and b) the second Paranal campaign.

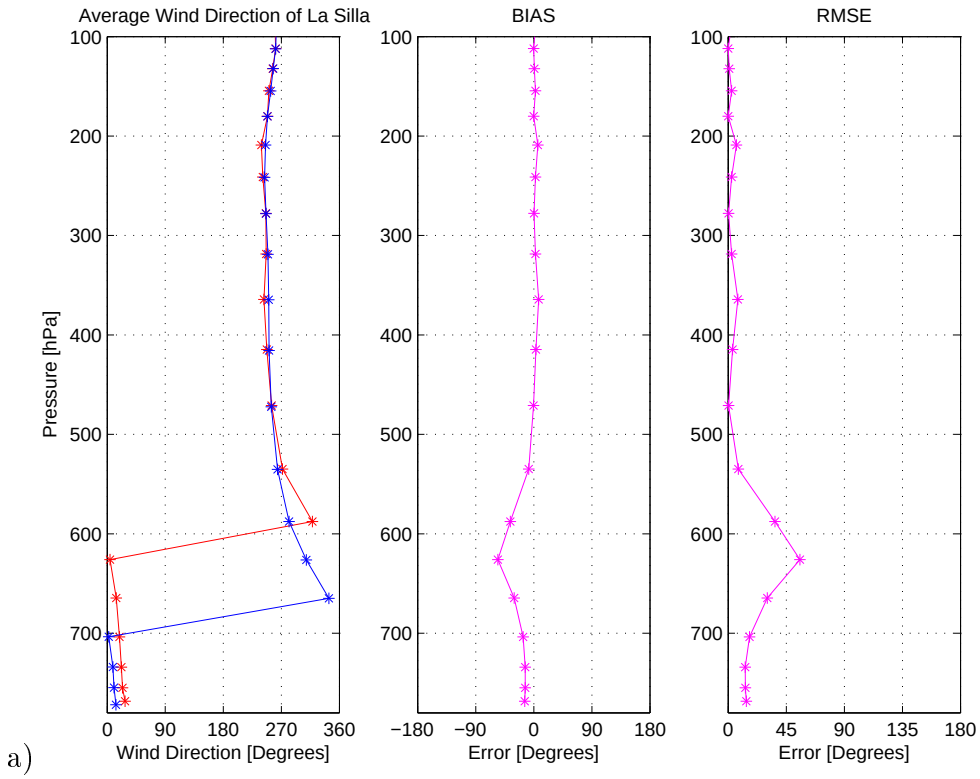

Figure 6.13: Mean vertical profiles of wind direction for radiosondes (red line) and WRF model (blue line) (first box), vertical profiles of BIAS (second box) and RMSE (third box) during a) La Silla campaign and b) APEX campaign.

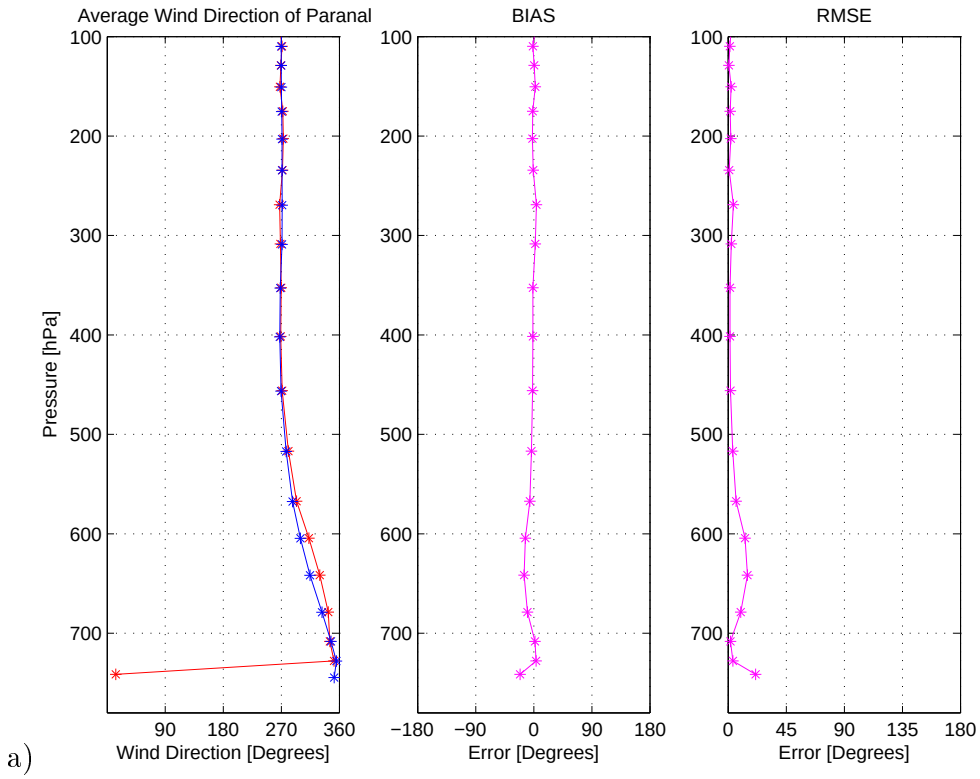

a)

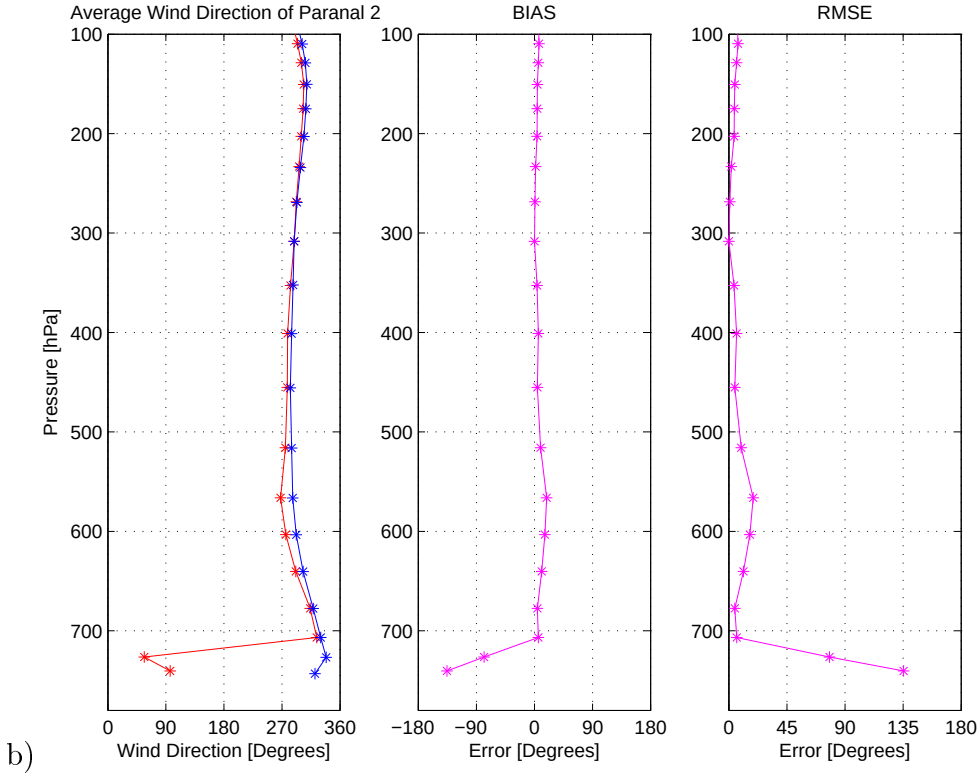

b)

Figure 6.14: Mean vertical profiles of wind direction for radiosondes (red line) and WRF model (blue line) (first box), vertical profiles of BIAS (second box) and RMSE (third box) during a) the first Paranal campaign and b) the second Paranal campaign.

Chapter 7

Synoptic study

In this section, a study of synoptic patterns present during the four campaigns is accomplished with the aim of identifying any correlation between large-scale atmospheric conditions and the PWV evolution obtained from radiosondes.

7.1 Data Set

The different data sources used in this section are described in table 7.2:

Source		**Data**	**Period**
Weather Station	La Silla	Temperature, Pressure, Relative Humidity, Wind Speed and Direction	May 5^{th} to 15^{th} of 2009
	Paranal	Temperature, Pressure, Relative Humidity, Wind Speed and Direction	July 29^{th} to August 10^{th} and November 9^{th} to 19^{th} of 2009
	APEX	Temperature, Pressure, Relative Humidity and Wind Speed	July 7^{th} to 16^{th} of 2009
Radiometer		PWV (Only for APEX campaigns)	24 hours from July 7^{th} to 16^{th} of 2009
Satellite Images		Visible (0.55 - 0.75 μm), Infrared (10.2 - 11.2 μm) and Water Vapor (6.5 - 7 μm)	May 5^{th} to 15^{th}, July 7^{th} to 16^{th}, July 29^{th} to August 10^{th} and November 9^{th} to 19^{th} of 2009
WRF		Temperature, wind vector, relative humidity and geopotencial fields from domain 1	output at 00, 06, 12 and 18 UTC for May 5^{th} to 15^{th}, July 7^{th} to 16^{th}, July 29^{th} to August 10^{th} and November 9^{th} to 19^{th} of 2009

Table 7.2: Data used in the synoptic study.

7.2 Synoptic patterns

The synoptic patterns analyzed are the same than those presented in the study of Macón, a preselected hill to install the E-ELT observatory [1] [4] and in the final ESO project report: "Study of Precipitable Water Vapor (PWV) at Llano de Chajnantor".

The synoptic patterns identified in the four campaigns were: Anticyclonic Predominance (**AP**), High Trough (**HT**), Cut-off Low (**CL**), Altiplanic Winter (**AW**) and Jet Stream (**JS**). In addition, combinations of two synoptic patterns (e.g. **AP**/**JS**, **HT**/**JS**) are also found.

The four campaigns were individually analyzed since they were scheduled on different seasons of the year.

7.2.1 First Campaign: La Silla Observatory

Eighteen radiosondes were launched during 11 days in May, the last autumn month. Four synoptic patterns were identified during this period: Anticyclonic Predominance (**AP**), High Trough (**HT**), Jet Stream (**JS**) and Cut-off Low (**CL**).

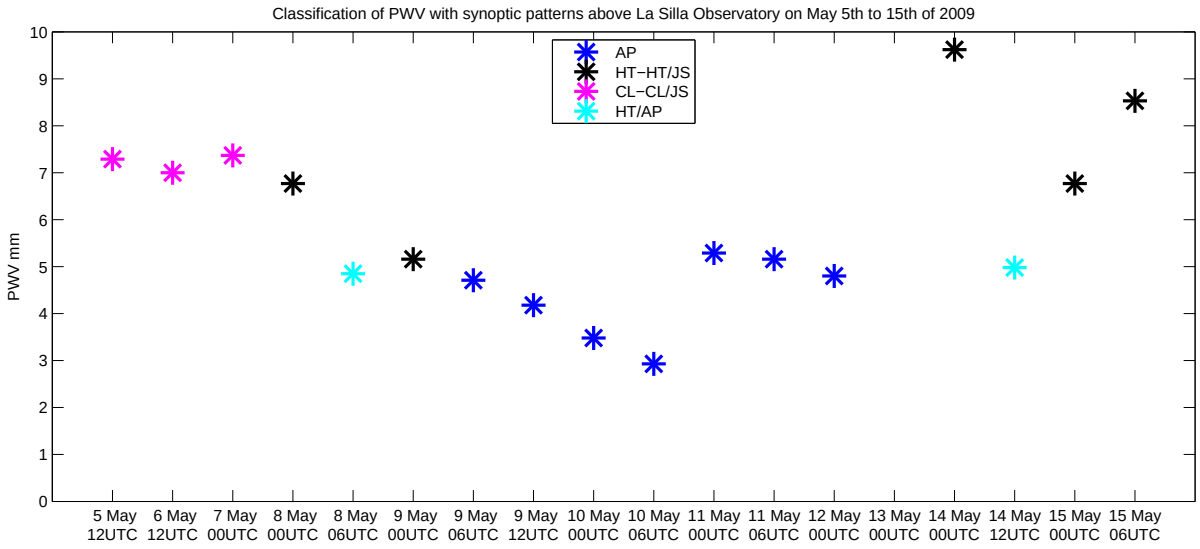

Figure 7.1: Synoptic patterns associated to each PWV value measured by radiosondes above La Silla Observatory.

Figure 7.1 shows the time series of PWV measured by radiosondes where each color is associated to the predominant synoptic pattern at that hour. During the first three days the presence of

[1] European Extremely Large Telescope.

CL is associated to relatively large values of PWV (average of 7.2 mm). Figure 7.2 shows a large water vapor contribution in the water vapor satellite image (Figure 7.2a). The dew-point and temperature vertical profiles measured by the radiosonde (Figure 7.2b) shows a moist layer between 500 hPa and 400 hPa associated to cloud formation. The WRF model shows a typical geopotential field associated to **CL** with large RH values at its front (Figure 7.2c). Figure 7.3 shows the water vapor mixing ratio vertical profile above La Silla at that time where the largest contribution to PWV is observed from the surface to 550 hPa with water vapor being almost constant over that layer.

Another synoptic pattern present in this campaign was **HT**, which was related to large values of PWV, showing an average of 6.65 mm. This configuration was identified in four different days, including May 14^{th}at 00 UTC, when the highest value of PWV (9.6 mm) was observed on this campaign. The water vapor satellite image at that time (Figure 7.4a) shows a relatively moist mid to high level layer above La Silla but it is drier than that in figure 7.2a. The radiosonde (figure 7.4b) shows a moist layer at higher levels with clouds presence but the largest contribution to PWV was observed near the surface (figure 7.3). At that day, much larger values were shown from the surface to almost 700 hPa than in May 6. Figure 7.4c shows a typical geopotential field present with a **HT** configuration near La Silla.

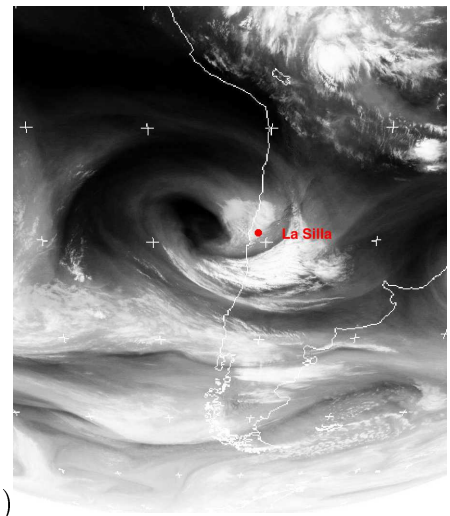

a)

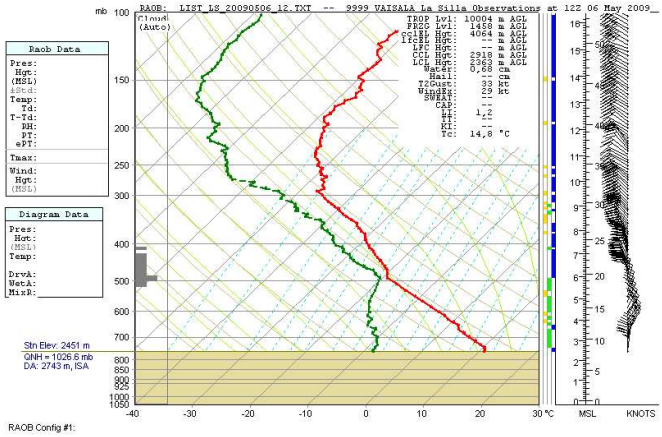

b)

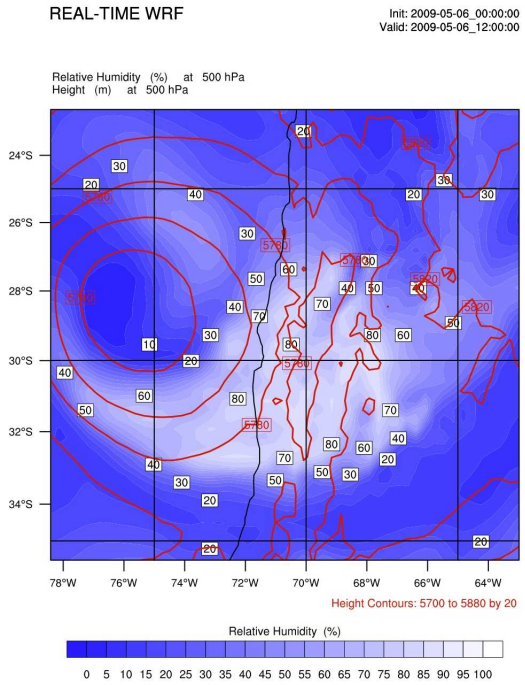

c)

Figure 7.2: May 6^{th} at 12 UTC, a) GOES-12 Water Vapor image, b) radiosonde and c) WRF model at 500 hPa.

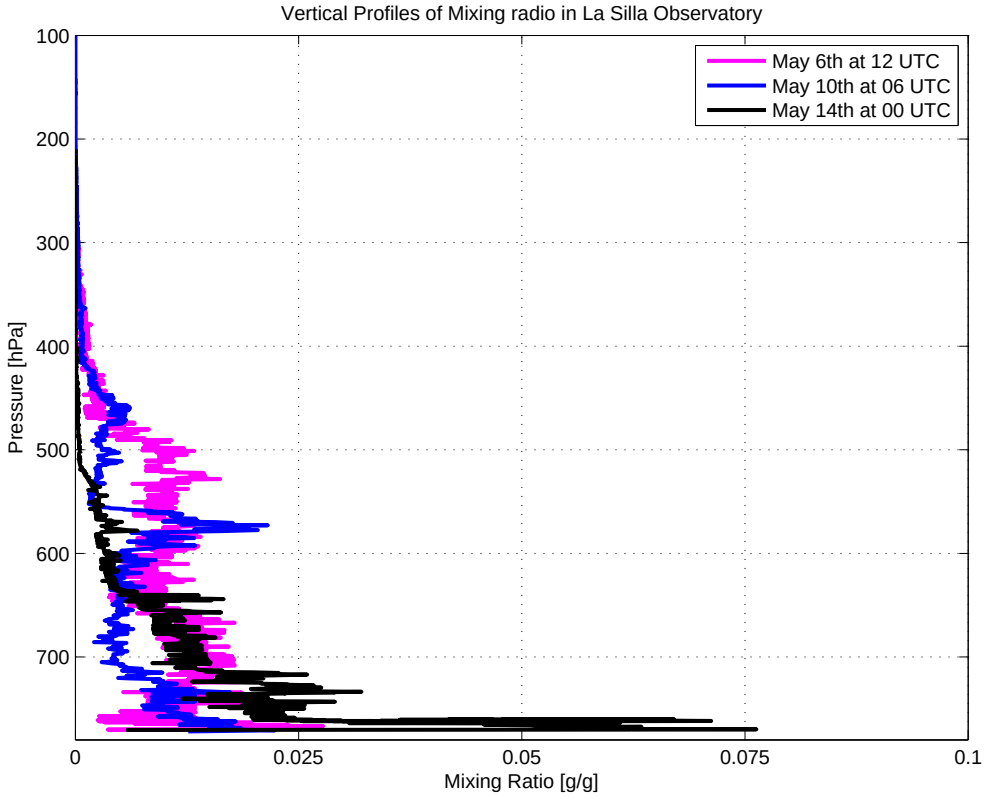

Figure 7.3: Vertical profiles of Mixing Radio above La Silla during May 6^{th} at 12 UTC, May 10^{th}at 06 UTC and May 14^{th} at 00 UTC.

At the times when the **AP** configuration is identified over La Silla site, the lowest values of PWV are shown 7.1. The water vapor satellite image (Figure 7.5a) shows a drier layer than that present in the previous analyzed days. The temperature vertical profiles (Figure 7.5b) and the water vapor mixing ratio profile indicate the presence of a drier atmosphere on that day where the largest contribution to PWV was shown in thin layers near the surface and between 600 and 550 hPa.

Figure 7.6 shows the histogram of the number of synoptic patterns found during the first campaign at La Silla observatory. The **AP** configuration was more frequent during this campaign although it was associated to relatively low values of PWV. Relatively large values of PWV were associated to **HT**, **HT/AP** and **CL** configurations.

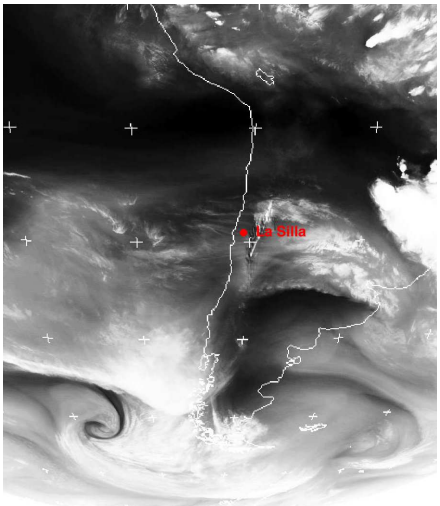

a)

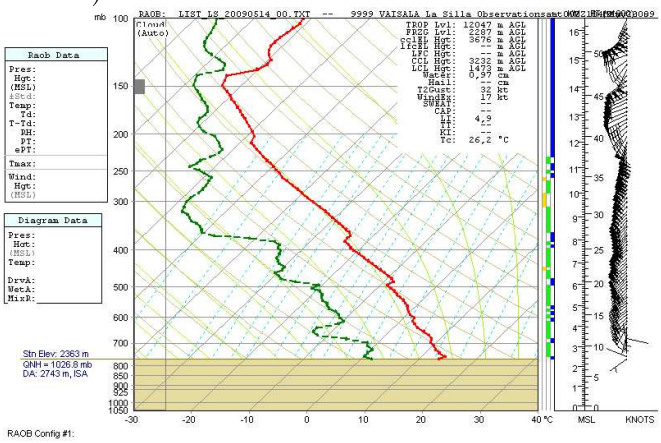

b)

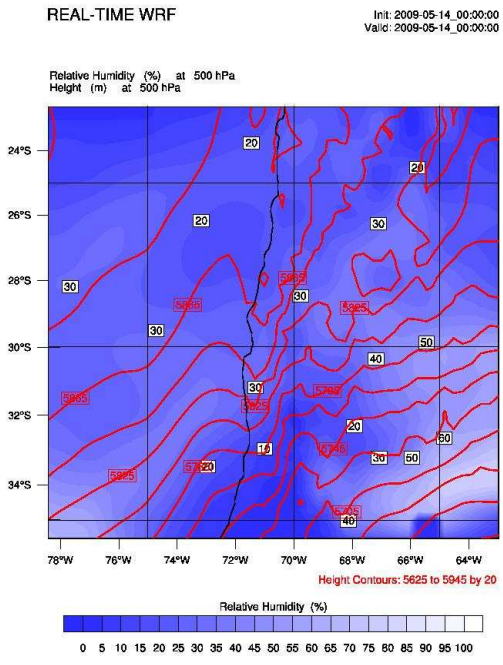

c)

Figure 7.4: May 14$^{\text{th}}$ at 00 UTC, a) GOES-12 Water Vapor image, b) radiosonde and c) WRF model at 500 hPa.

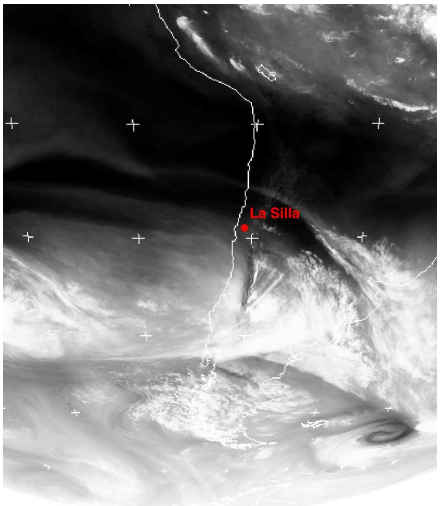

a)

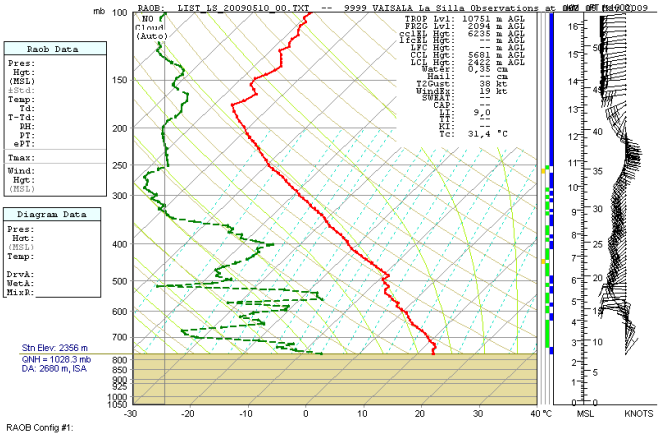

b)

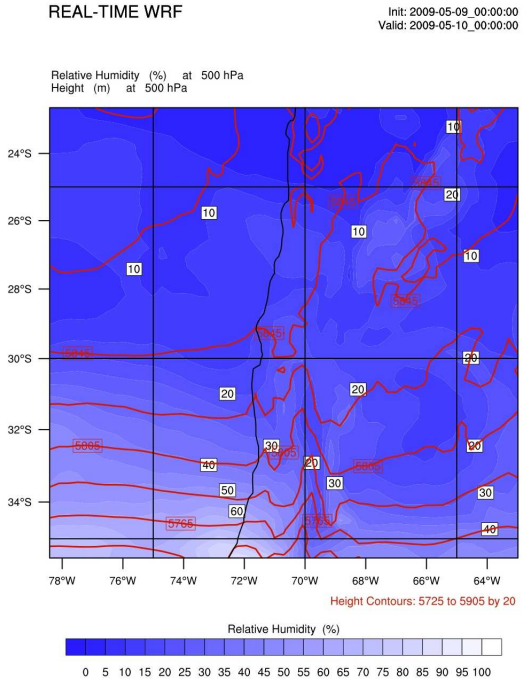

c)

Figure 7.5: May 10th at 00 UTC, a) Water Vapor image, b) radiosonde and c) WRF model at 500 hPa.

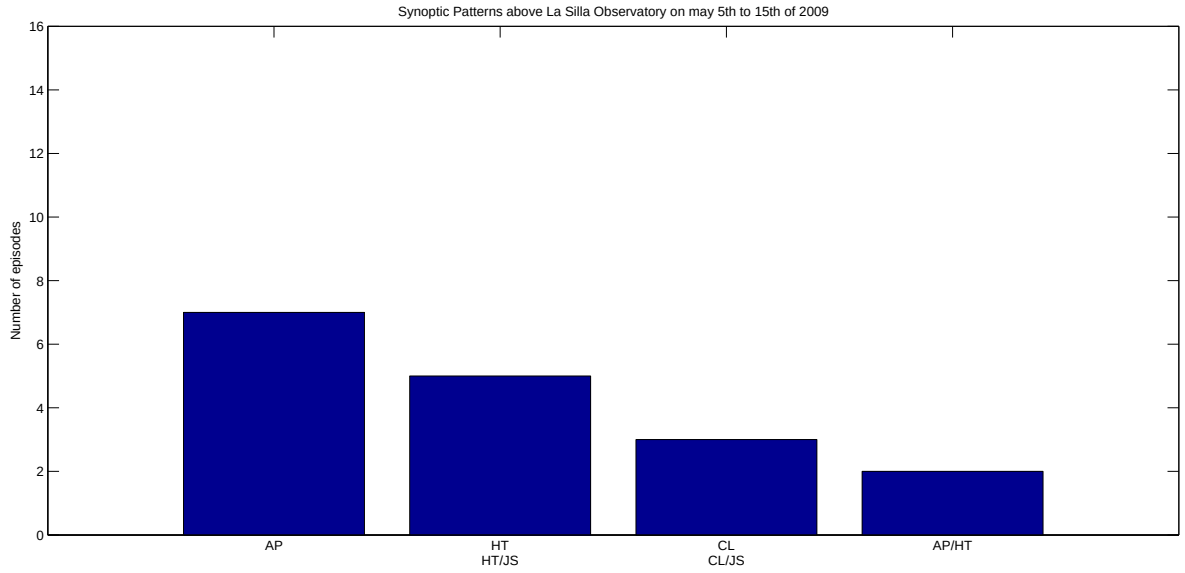

Figure 7.6: Histogram of the synoptic pattern over La Silla Observatory.

7.2.2 Second Campaign: APEX Observatory

Twenty radiosondes were launched during 10 days in July, the first winter month. Three synoptic patterns were identified during this period: Anticyclonic Predominance (**AP**), Jet Stream (**JS**) and Cut-off Low (**CL**). As mentioned in section 3.2, the location where radiosondes were launched moved to San Pedro de Atacama in the middle of APEX campaign. However, the analysis was focused on APEX location.

Figure 7.7 shows the predominant synoptic pattern associated to each PWV value measured by radiosondes. The presence of **AP** was identified from July 7^{th} to July 12^{th} associated to low values of PWV. Figure 7.8a shows the GOES water vapor image for July 7^{th} at 00 UTC where dry conditions are indicated above APEX. This is also shown on the dew-point and temperature vertical profiles from radiosondes where a dry atmosphere is observed at that time (figure 7.8b). The **JS** configuration combines with AP (**AP**/**JS**) from July 9^{th} to 12^{th} but only a slightly increase in PWV was observed (Figure 7.7).

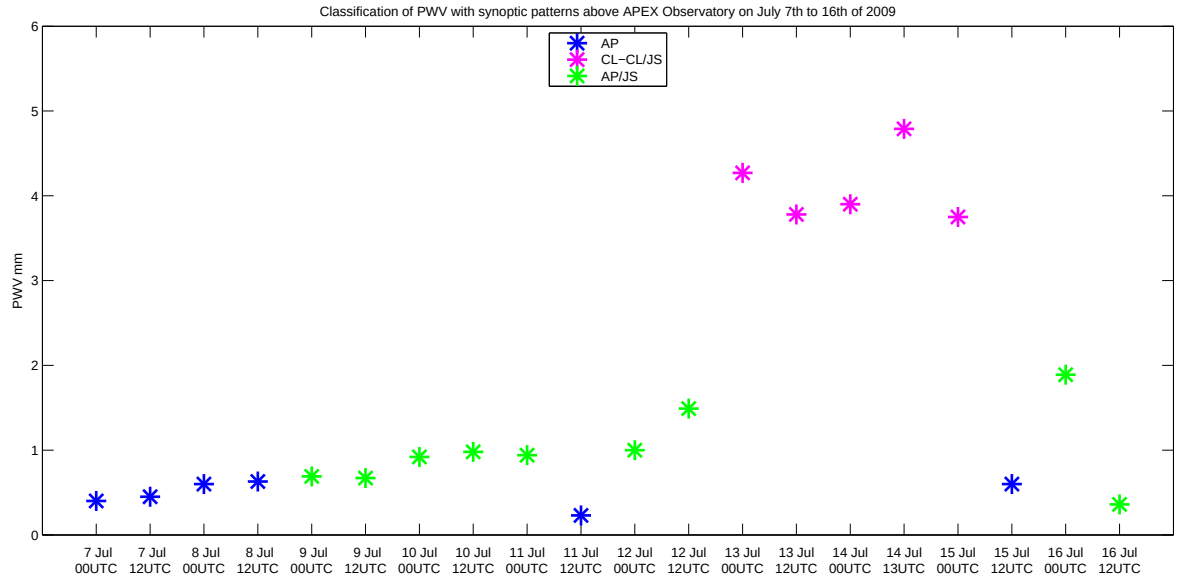

Figure 7.7: Synoptic patterns associated to each PWV value measured by radiosondes on APEX Observatory.

The presence of **CL** was identified from July 13^{th} at 00 UTC to July 15^{th} at 00 UTC associated to larger values of PWV. The average PWV over these days was 4.1 mm with near-surface relative humidity values ranging between 45% and 96% and wind speeds larger than 15 m/s. The influence of a relatively moist mid to high-level layer above APEX is observed in the GOES water vapor satellite image for July 14^{th} at 12 UTC (Figure 7.9a). At that time, the temperature profiles show a saturated layer from the surface to 350 hPa associated to clouds formation (Figure 7.9b). Large RH values were simulated by WRF at 500 hPa (Figure 7.9). After July 15^{th}, **AP** and **AP/JS** were identified, associated to dry conditions and a low contribution of water vapor (Figure 7.7).

Figure 7.10 shows the histogram of the number of times synoptic patterns were found during the APEX campaign. The **AP** configuration predominated during the APEX campaign with **AP/JS** and **AP** identified on 15 from a total of 20 radiosondes launches. Those configurations showed the lowest values of PWV with an average of 0.99 mm (**AP/JS**) and 0.49 mm (**AP**). The largest values of PWV were observed during the presence of **CL** with an average PWV of 4.1 mm.

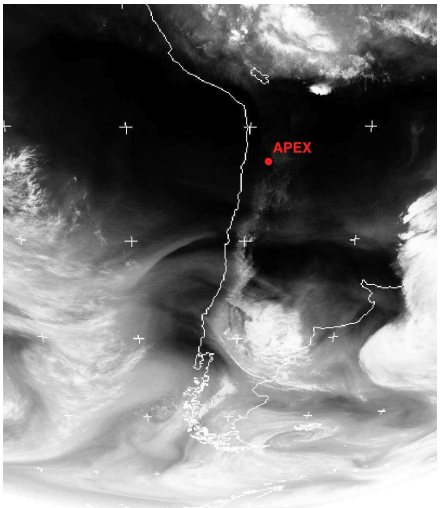

a)

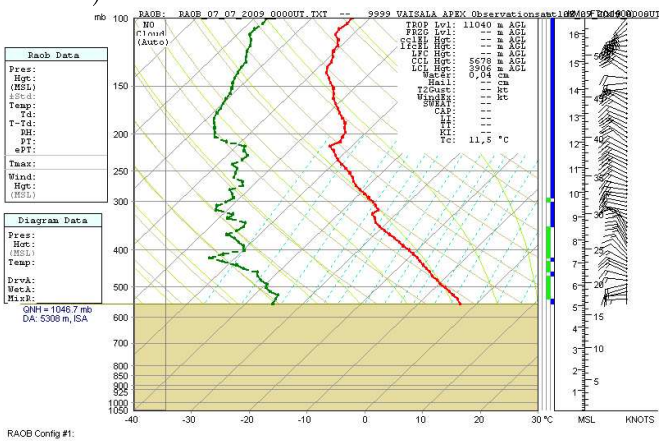

b)

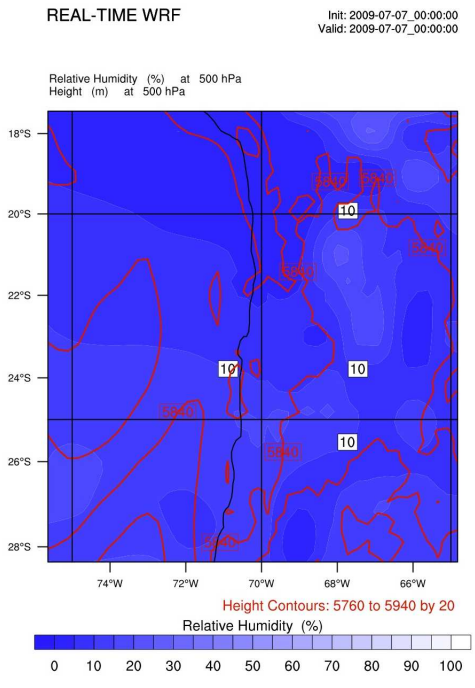

c)

Figure 7.8: July 7$^{\text{th}}$ at 00 UTC, a)GOES-12 Water Vapor image, b) radiosonde and c) WRF model at 500 hPa., radiosonde, satellite image and model WRF.

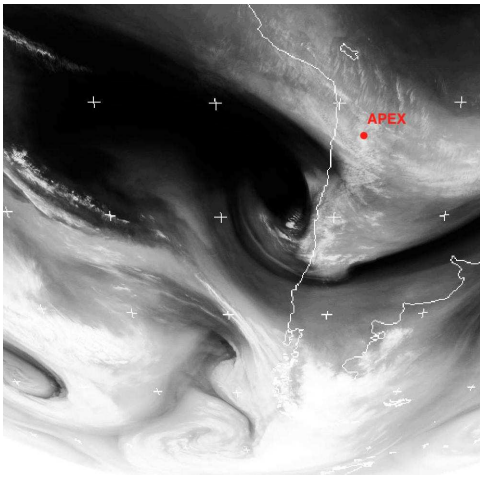

a)

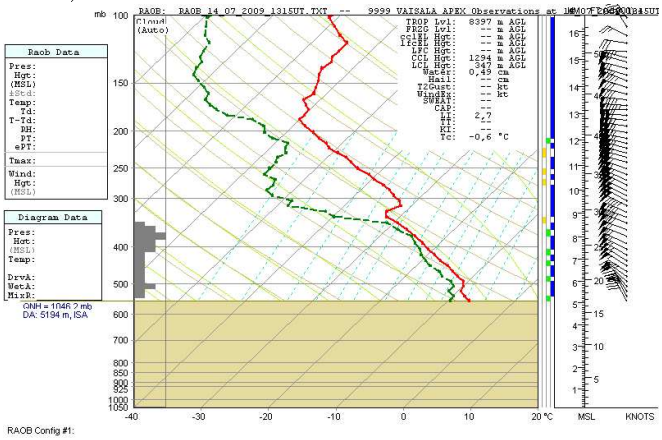

b)

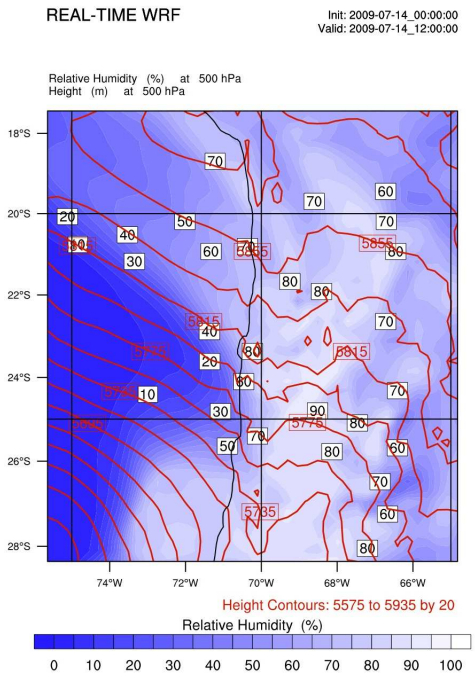

c)

Figure 7.9: July 14th at 12 UTC, a)GOES-12 Water Vapor image, b) radiosonde and c) WRF model at 500 hPa.

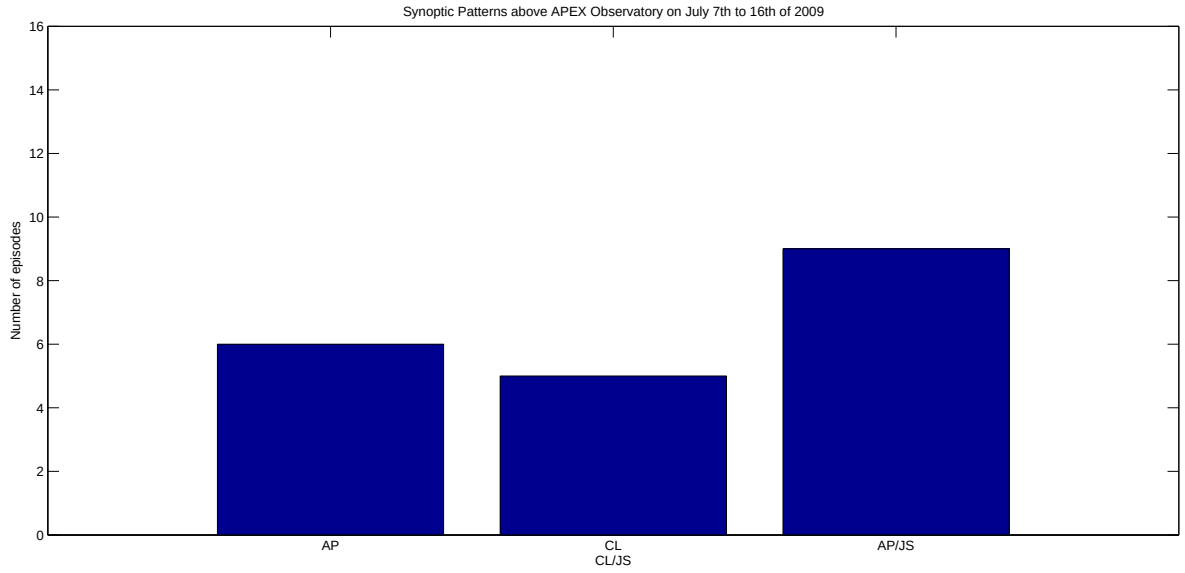

Figure 7.10: Histogram of the synoptic pattern over APEX Observatory.

7.2.3 Third Campaign: Paranal Observatory

This campaign was conducted during the winter season at Paranal. Twenty three radiosondes were launched during the last three days of July and the first 10 days of August (Table 3.3). Four synoptic patterns were identified during this period: Anticyclonic Predominance (**AP**), High Trough (**HT**), Jet Stream (**JS**) and Cut-off Low (**CL**).

Figure 7.11 shows the time series of PWV measured by radiosondes at Paranal site, where each color is related to the predominant synoptic pattern at the radiosonde launch time. Two synoptic patterns are associated to a rapid increase in PWV, **HT/JS** and **CL**.

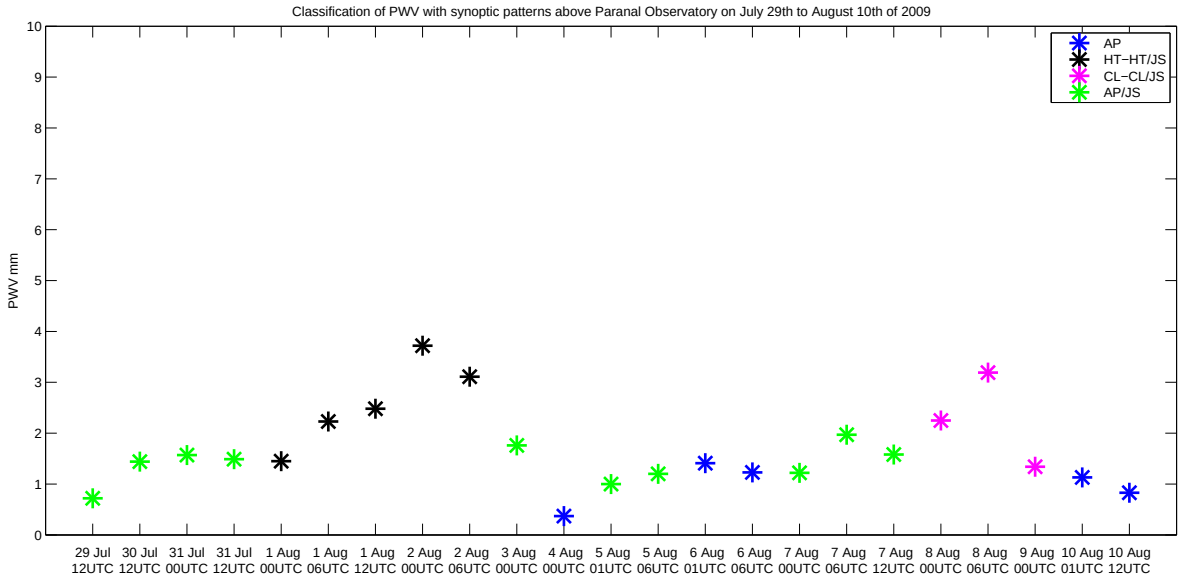

Figure 7.11: Synoptic patterns associated to each PWV value measured by radiosondes on Paranal Observatory.

A rapid increase in PWV was observed from August 1^{st} at 00 UTC to August 2^{nd} at 00 UTC, associated to **HT/JS** pattern. Figure 7.12a shows the water vapor satellite image for August 2^{nd} at 00 UTC, where the largest PWV value (3.72 mm) was observed. A certain amount of humidity is present above Paranal but no clouds were identified from the radiosonde profile (Figure 7.12b).

Another PWV increase was observed from August 7^{th} at 06 UTC to August 8^{th} at 00 UTC mainly associated to **CL** and **CL/JS** reaching a PWV value larger than 3 mm.

The lowest value of PWV (0.4 mm) during the campaign is present on August 4^{th} at 00 UTC. The water vapor image at that time (Figure 7.13a) shows a much drier mid to higher level layer than that at August 2^{nd} at 00 UTC, indicating the presence of **AP** pattern. The temperature vertical profiles from the radiosonde shows a much drier atmosphere, particularly below 400 hPa (Figure 7.13b).

Figure 7.14 shows the histogram of the number of times synoptic patterns were identified in this campaign. The **AP** pattern (**AP** and **AP/JS**) predominated over the third campaign mainly associated to relatively low values of PWV. The **HT-HT/JS** and **CL-CL/JS** were found less times but related to a PWV increase.

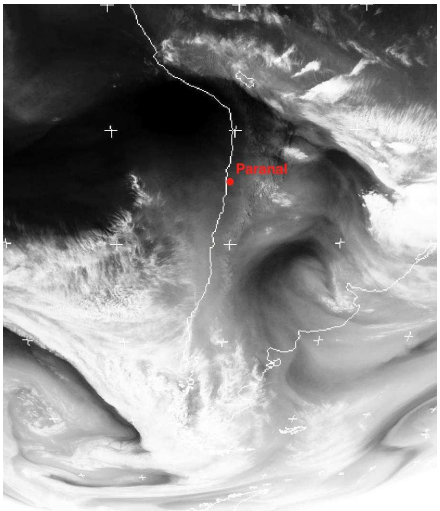

a)

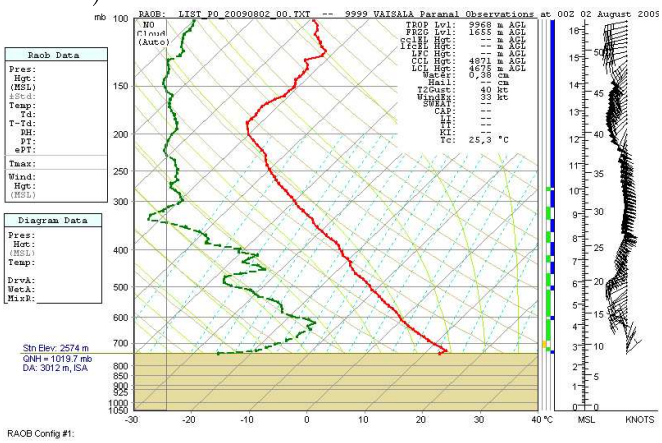

b)

c)

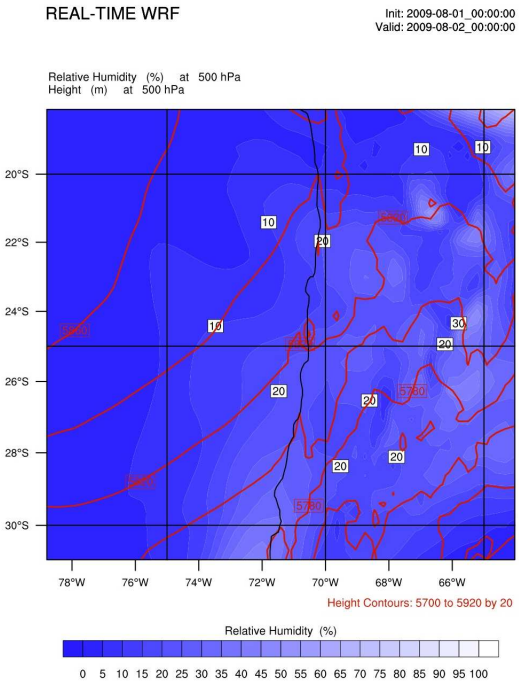

Figure 7.12: August 2^{nd} at 00 UTC, a) GOES-12 Water Vapor image, b) radiosonde and c) WRF model at 500 hPa.

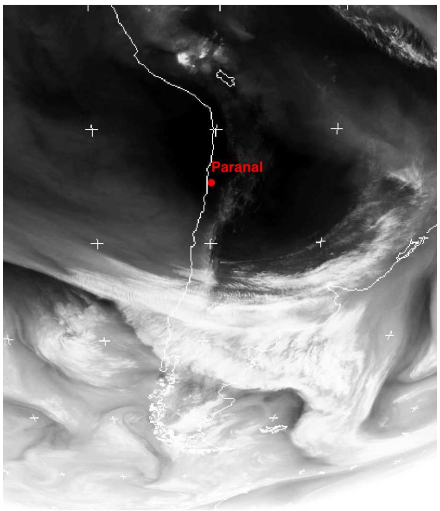

a)

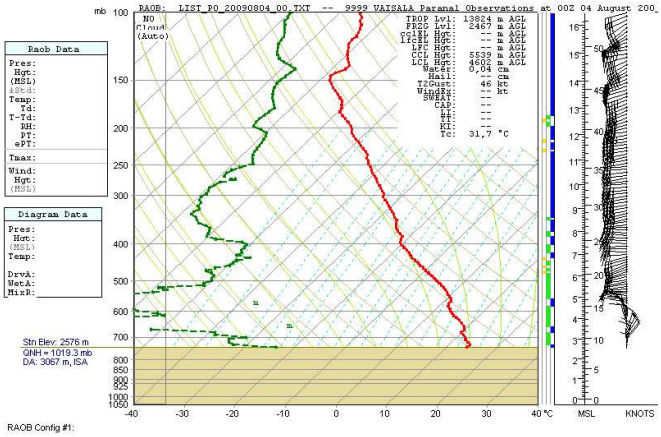

b)

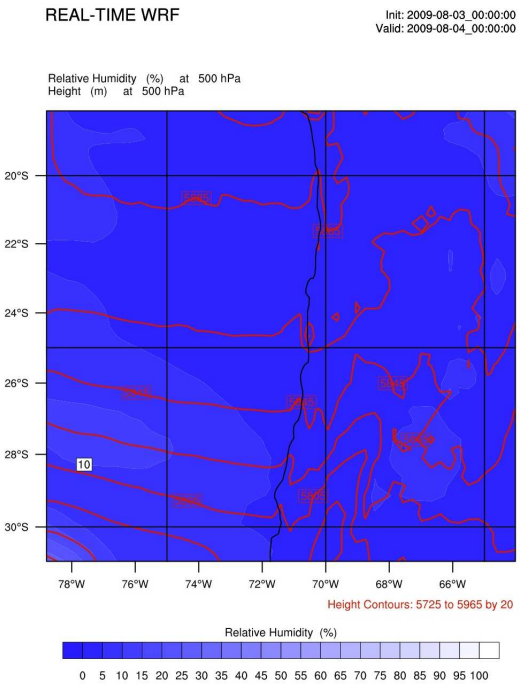

c)

Figure 7.13: August 4^{th} at 00 UTC, a) Water Vapor image, b) radiosonde and c) WRF model at 500 hPa.

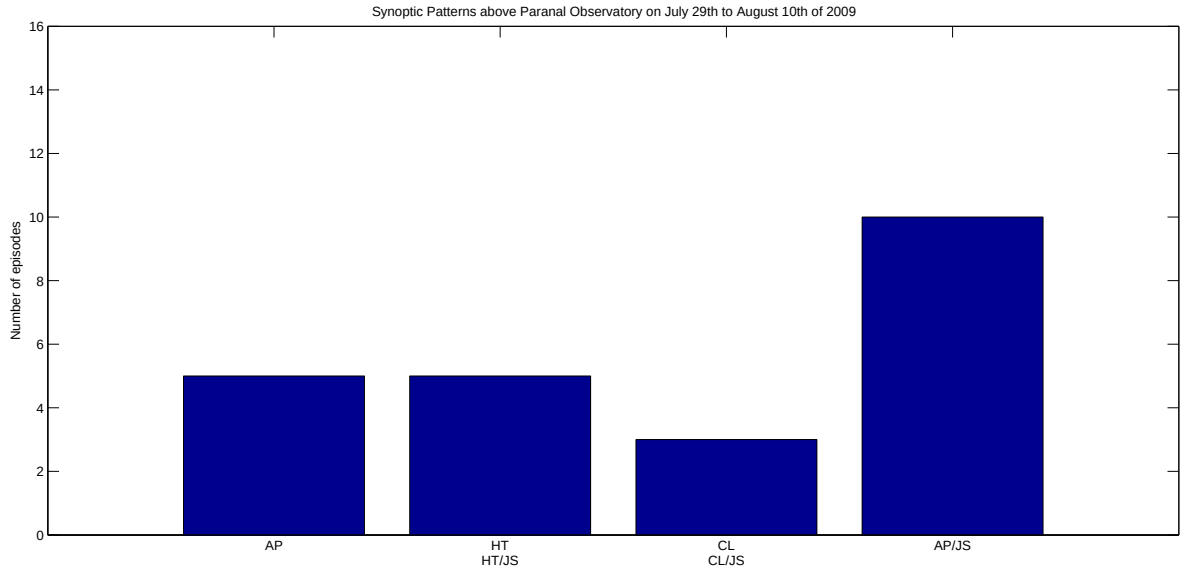

Figure 7.14: Histogram of the number of times synoptic patterns were found Paranal Observatory.

7.2.4 Fourth Campaign: Paranal Observatory

Twenty nine radiosondes were launched during 11 days in November (Table 3.3), the last spring month. Four synoptic patterns were identified during this period: Anticyclonic Predominance (**AP**), High Trough (**HT**), Jet Stream (**JS**) and Altiplanic Winter (**AW**).

Figure 7.15 shows the time series of PWV for this campaign where each color is associated to the predominant synoptic pattern at each hour. During this campaign, the PWV shows little variability although **AP** and **AP/JS** are related to relatively small values of PWV.

The synoptic pattern related to relatively large PWV values was **HT/JS**, with a value of 3.03 mm observed on November 9^{th} at 12 UTC (Figure 7.16). On that day, figure 7.16a shows the presence of water vapor from middle to higher levels of the atmosphere but no clouds are indicated from the radiosonde temperature profiles (Figure 7.16b).

On November 14^{th} at 12 UTC, the lowest PWV value (1.1 mm) was measured during **AP/JS** presence. Figure 7.17a shows the presence of water vapor from mid to higher levels. A relatively moist layer is indicated in temperature vertical profiles from the radiosonde (Figure 7.17b). However, a much drier layer is observed from the surface to 300 hPa, corroborating the low PWV value at that time.

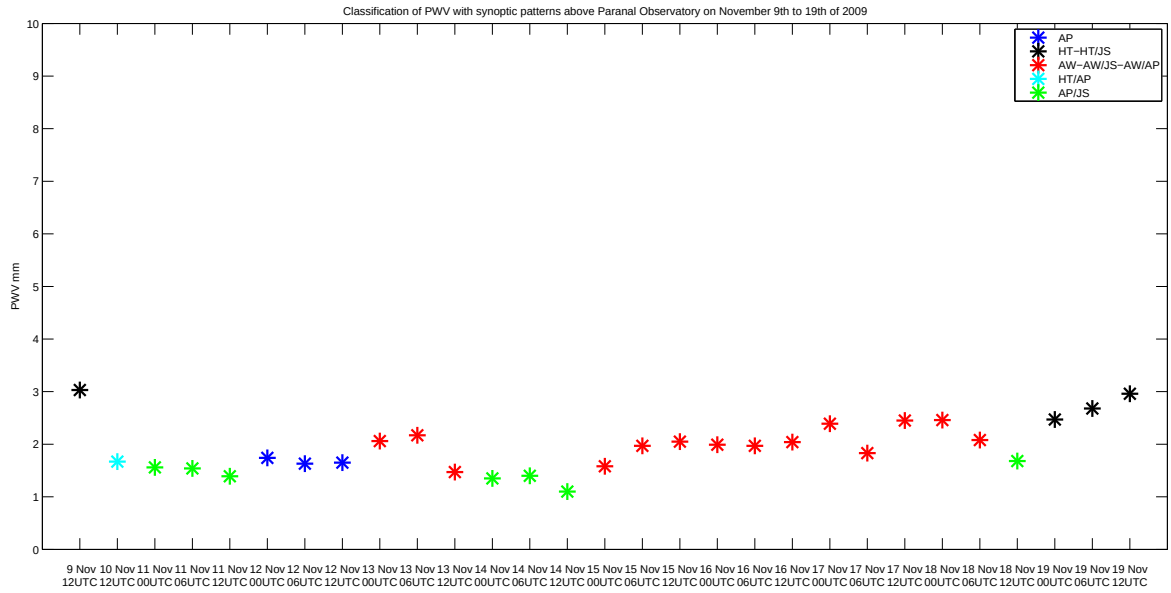

Figure 7.15: Classification of PWV measured by the radiosondes with synoptic patterns above Paranal Observatory.

A small and sustained increase in PWV is observed from November 15^{th} at 00 UTC to November 18^{th} at 00 UTC under the influence of **AW** pattern. A relative large value of 2.45 mm is observed on November 17^{th} at 00 UTC. Figure 7.18a shows moist conditions over Paranal from middle to higher levels. A relatively moist layer is indicated from radiosonde profiles (7.18b) between 400 hPa and 200 hPa with the presence of clouds. However, an extremely dry layer is observed below cloud, causing PWV not to increase too much.

Figure 7.19 shows the frequency of occurrence of synoptic patterns during the campaign, where **AW** and **HT** predominated with relatively high values of PWV (1.78 mm and 2.79 mm, respectively).

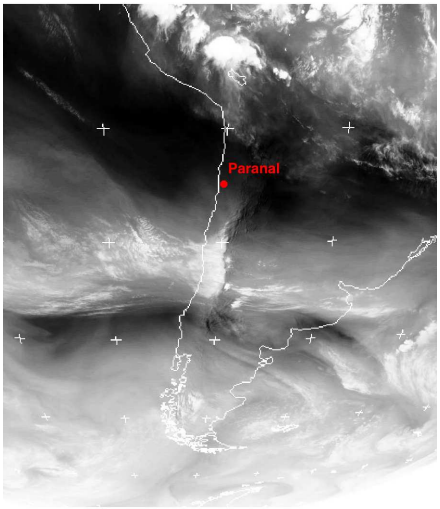

a)

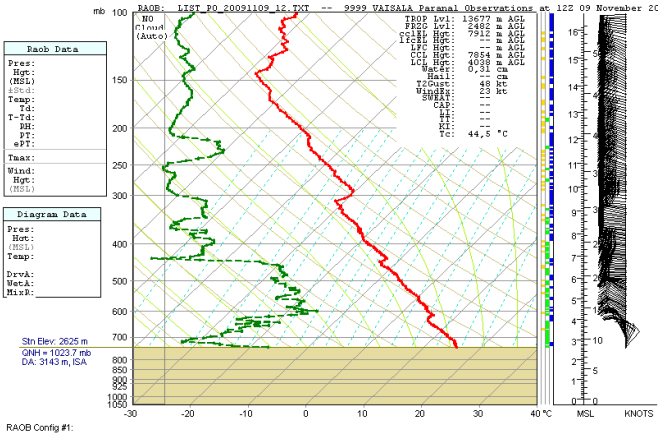

b)

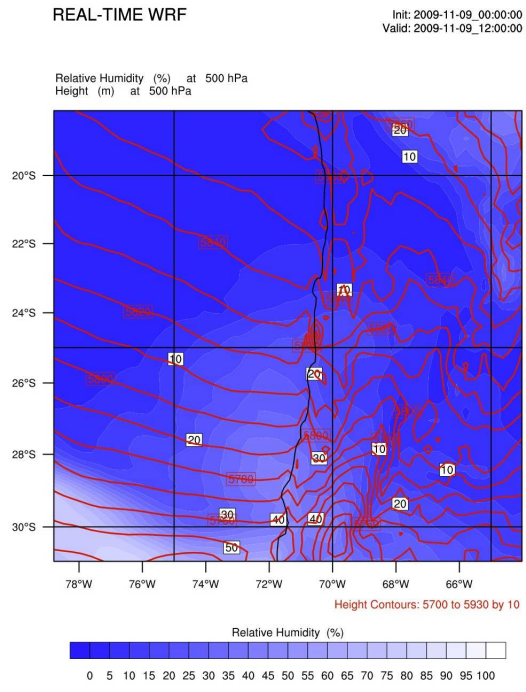

c)

Figure 7.16: November 9^{th} at 12 UTC, a) GOES-12 Water Vapor image, b) radiosonde and c) WRF model at 500 hPa.

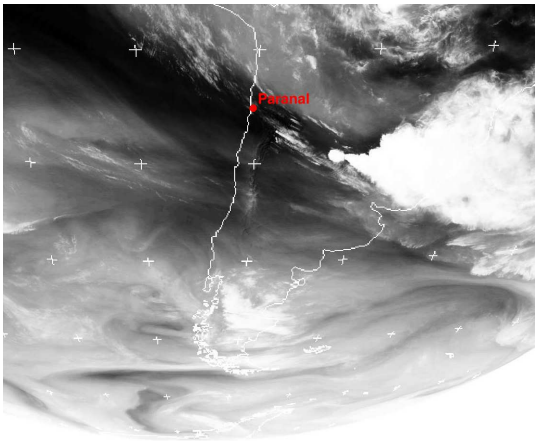

a)

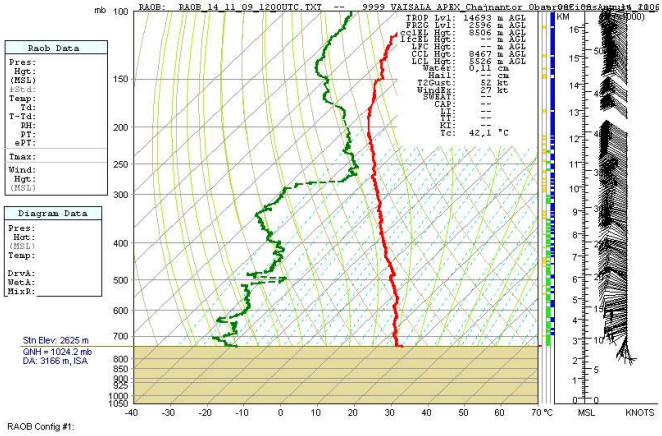

b)

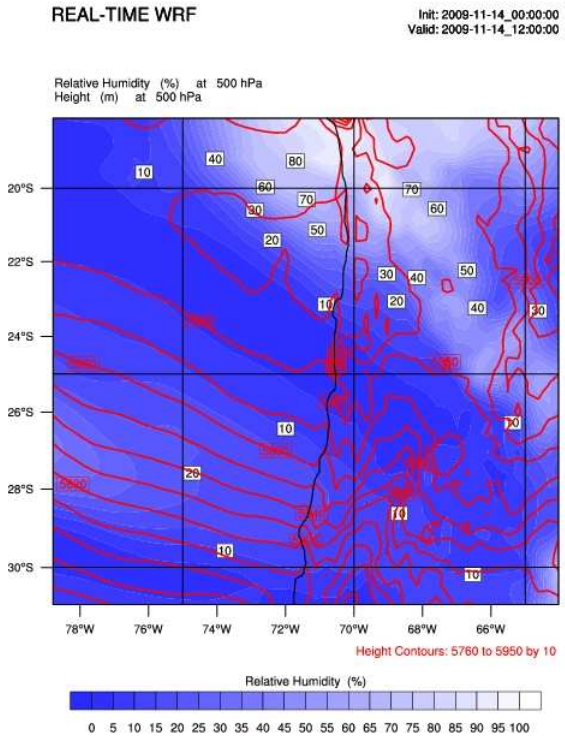

c)

Figure 7.17: November 14^{th} at 12 UTC, a)GOES-12 Water Vapor image, b) radiosonde and c) WRF model at 500 hPa.

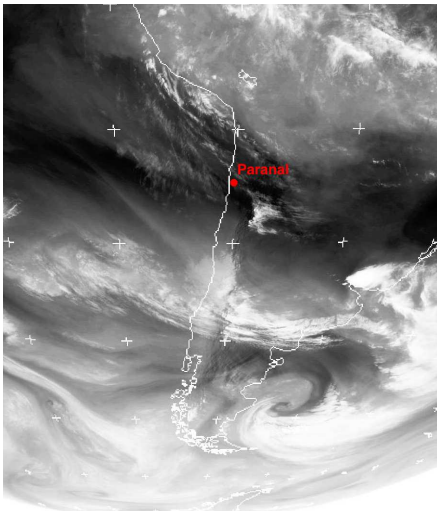

a)

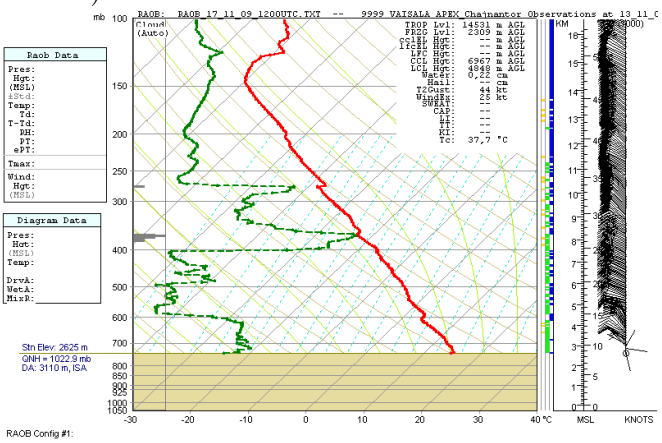

b)

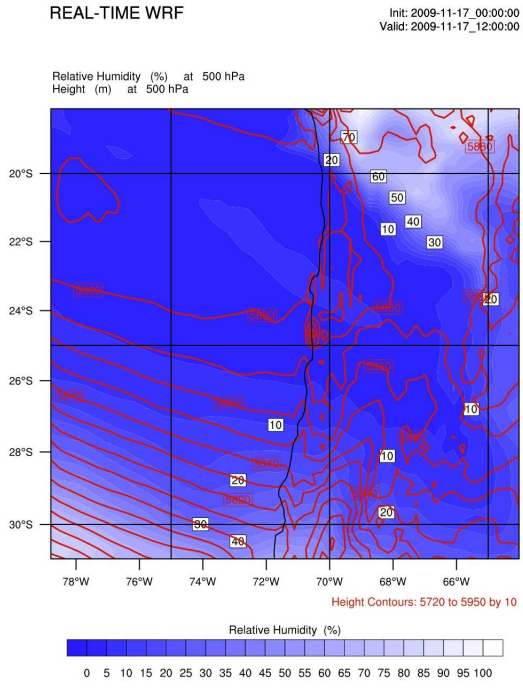

c)

Figure 7.18: November 17^{th} at 12 UTC, a) Water Vapor image, b) radiosonde and c) WRF model at 500 hPa.

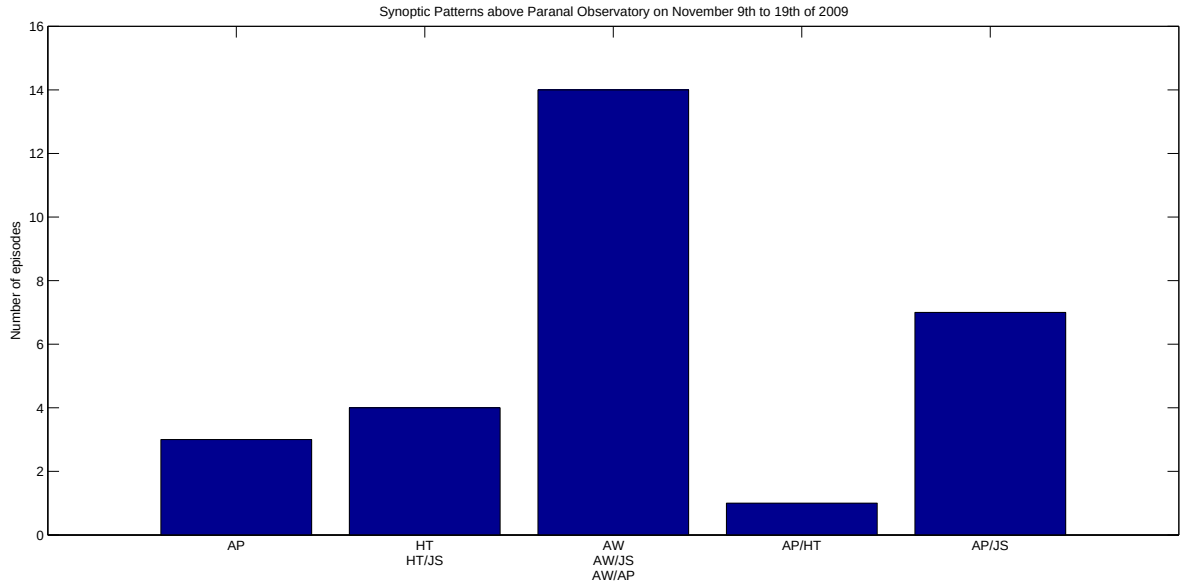

Figure 7.19: Histogram of the synoptic pattern over Paranal Observatory.

Chapter 8

Conclusions

The radiosondes campaigns were successfully conducted on La Silla, APEX and Paranal observatories, obtaining good quality data. Radiosonde data were used to evaluate the performance of PWV estimations and forecasts obtained from two meteorological tools at each site.

The first evaluation was carried out on the estimation of PWV from GOES-12 satellite data and FNL analysis (GOES/FNL). The comparison with radiosondes shows that GOES/FNL overestimates PWV at the three sites. The best performance was obtained at APEX site although only a small number of GOES data were available for that period. Good results were also obtain at that site comparing with radiometer data as was shown on the project report: "Study of Precipitable Water Vapor (PWV) at Llano de Chajnantor".

The PWV estimation from GOES/FNL at La Silla and Paranal during autumn show larger errors than those obtained at APEX but the PWV variations during these campaigns were reproduced relatively well. On the other hand, the PWV estimation during the second Paranal campaign shows no correlation at all and large errors. The better agreement in APEX could be related to the fact that the methodology to obtain PWV from GOES was developed for APEX and later adapted to the other sites but the comparison over a much larger period needs to be done.

The WRF meteorological model was also evaluated with radiosondes, comparing the predicted PWV and several atmospheric vertical profiles. In the evaluation of PWV forecasts, the best agreement were obtained during the APEX campaign, showing very small errors. When comparing both Paranal campaigns, the best model performance was obtained during winter on the first campaign. A future study using a much larger time period could corroborate whether indeed the model shows a better agreement during the cold season than the warm season and why.

The analysis over La Silla and Paranal sites show larger errors than APEX. A possible explanation for this could be that APEX is located at ~5100 m of altitude, farther away from the coast than the other sites and with a smaller PWV seasonal variation. Another factor could be that the WRF configuration used on the three study sites is the best found for atmospheric conditions at APEX site. A future study could evaluate different configurations for La Silla and Paranal to obtain a better performance over each place.

The comparison of vertical profiles from WRF and radiosondes shows a good agreement in the four campaigns. In general, temperature and wind direction simulated profiles show good agreement at upper levels and the largest errors near the surface. This could be related to the fact that the three observatories are located over complex terrain. The water vapor mixing ratio is better reproduced at APEX site and is mostly overestimated at La Silla and Paranal, which also influences the PWV calculation over these sites. The simulated RH is overestimated at upper levels and wind speed is reproduced well at all levels and during the four campaigns.

Using WRF simulations, GOES-12 satellite images and radiosondes vertical profiles, the synoptic patterns present during each campaign were identified with the aim of identifying any correlation between large-scale atmospheric conditions and the PWV evolution. The synoptic patterns identified in the four campaigns were: Anticyclonic Predominance (**AP**), High Trough (**HT**), Cut-off Low (**CL**), Altiplanic Winter (**AW**) and Jet Stream (**JS**). In addition, combinations of two synoptic patterns (e.g. **AP/JS**, **HT/JS**) are also found. In general, **AP** was the synoptic pattern that predominated during most of the radiosonde launching times but was associated to a dry atmosphere with low PWV values. **AW** and **HT** were less frequent but were associated to periods of PWV increase and maximum PWV values.

Acknowledgements

The authors express appreciation to Florian Kerber and Marc Sarazin for truth in the Astrometeorology group to perform the radiosonde campaigns. To the staff of La Silla Observatory, specifically to Aldo Pizarro for his help in logistics. To the staff of APEX Observatory, specifically to David Rabanus who help to the transport and logistics, too. To the staff of Paranal Observatory, specifically to Gordon Gillet with all help in Logistics to. And for Direccion de Aeronáutica Civil (DGAC), to let us launch the radiosonde in the schedule made to develop the study.

REFERENCES

[1] Åkerberg J.: State-of-the-art radiosonde telemetry, Eighth Symposium on Integrated Observing ans Assimilation Systems for Atmosphere, Oceans and Land Surface, American Meteorological Society, 2004.

[2] http://amsglossary.allenpress.com/glossary/search?id=precipitable-water1

[3] Freund & Walpde, 1990: Estadística matemática con aplicaciones, Pearson 6º Edition, 2000.

[4] Cuevas, O., Chacón, A., Curé, M., 2008: Analysis of local meteorological conditions in Macón using the MM5 modeling system. Proceedings of the SPIE, volume 7016, pp. 701620-701620-12.

[5] http://www.arl.noaa.gov/fnl.php